Evaluating the Model Representation of Asian Summer Monsoon UTLS Transport and Composition using Airborne In Situ Observations

Warren P Smith[1], Laura L Pan[2], Douglas Edward Kinnison[3], Elliot L. Atlas[4], Shawn Honomichl[5], Jun Zhang[5], Simone Tilmes[6], Rafael Pedro Fernandez[7], Alfonso Saiz-Lopez[8], Victoria Treadaway[9], Karina E Adcock[10], Johannes C. Laube[11], M. von Hobe[12], Corinna Kloss[12], Silvia Viciani[13], Francesco D'Amato[14], C. Michael Volk[15], and Fabrizio Ravegnani[16]

[1]NCAR
[2]National Center for Atmospheric Research (NCAR)
[3]NCAR/CLAS
[4]RSMAS
[5]National Center for Atmospheric Research
[6]National Center for Atmospheric Research (UCAR)
[7]National Research Council (CONICET)
[8]Spanish National Research Council (CSIC)
[9]Cooperative Institute for Research in Environmental Sciences
[10]University of East Anglia
[11]Forschungszentrum Juelich GmbH
[12]Forschungszentrum Juelich
[13]CNR-INO National Institute of Optics
[14]CNR - Istituto Nazionale di Ottica
[15]University of Wuppertal
[16]CNR

August 4, 2023

Abstract

Chemistry transport models (CTMs) are essential tools for characterizing and predicting the role of atmospheric composition and chemistry in Earth's climate system. This study demonstrates the use of airborne in situ observations to diagnose the representation of atmospheric composition by global CTMs. Process-based diagnostics are developed which minimize the spatial and temporal sampling differences between airborne in situ measurements and CTM grid points. The developed diagnostics make use of dynamical and chemical vertical coordinates as a means of highlighting areas where focused model improvement is needed. The chosen process is the chemical impact of the Asian summer monsoon (ASM), where deep convection serves a unique pathway for rapid transport of surface emissions and pollutants to the stratosphere. Two global CTM configurations are examined for their representation of the ASM upper troposphere and lower stratosphere (UTLS), using airborne observations collected over south Asia. Application of the developed diagnostics to the CTMs reveals the limitations of zonally-averaged surface boundary conditions for species with sufficiently short tropospheric lifetimes, and that species whose stratospheric loss rates are dominated by photolysis have excellent agreement compared to that observed. Overall, the diagnostics demonstrate

the strength of airborne observations toward improving model predictions, and highlight the utility of highly-resolved CTMs to improve the understanding of reactive transport of anthropogenic pollutants to the stratosphere.

Evaluating the Model Representation of Asian Summer Monsoon UTLS Transport and Composition using Airborne In Situ Observations

Warren P. Smith[1], Laura L. Pan[1], Douglas Kinnison[1], Elliot Atlas[2], Shawn Honomichl[1], Jun Zhang[1], Simone Tilmes[1], Rafael P. Fernandez[3], Alfonso Saiz-Lopez[4], Victoria Treadaway[5,6], Karina E. Adcock[7], Johannes C. Laube[8], Marc von Hobe[8], Corinna Kloss[8], Silvia Viciani[9], Francesco D'Amato[9], C. Michael Volk[10], Fabrizio Ravegnani[11]

[1]Atmospheric Chemistry Observations & Modeling Laboratory, National Center for Atmospheric Research, Boulder, Colorado, USA
[2]Department of Atmospheric Sciences, Rosenstiel School of Marine, Atmospheric, and Earth Science, University of Miami, Miami, Florida, USA
[3]Institute for Interdisciplinary Science (ICB), National Research Council (CONICET), FCEN-UNCuyo, Mendoza, Argentina
[4]Department of Atmospheric Chemistry and Climate, Institute of Physical Chemistry Blas Cabrera, CSIC, Madrid, Spain
[5]Cooperative Institute for Research in Environmental Sciences, University of Colorado Boulder, Boulder, Colorado, USA
[6]NOAA Chemical Sciences Laboratory, Boulder, Colorado USA
[7]Centre for Ocean and Atmospheric Sciences, School of Environmental Sciences, University of East Anglia, Norwich, UK
[8]Institute for Energy and Climate Research (IEK-7), Forschungszentrum Jülich GmbH, 52425 Jülich, Germany
[9]National Research Council - National Institute of Optics (CNR-INO), Sesto Fiorentino, Italy
[10]University of Wuppertal, Germany
[11]Institute of Atmospheric Sciences and Climate, Bologna, Italy

Key Points:

- We develop process-based diagnostics for model evaluation using airborne in situ observations
- We analyze the representation of the Asian summer monsoon for its role in impacting composition and climate
- The established diagnostics use dynamical and chemical coordinates to identify areas for model improvement

Corresponding author: Warren P. Smith, `wsmith@ucar.edu`

Abstract

Chemistry transport models (CTMs) are essential tools for characterizing and predicting the role of atmospheric composition and chemistry in Earth's climate system. This study demonstrates the use of airborne in situ observations to diagnose the representation of atmospheric composition by global CTMs. Process-based diagnostics are developed which minimize the spatial and temporal sampling differences between airborne in situ measurements and CTM grid points. The developed diagnostics make use of dynamical and chemical vertical coordinates as a means of highlighting areas where focused model improvement is needed. The chosen process is the chemical impact of the Asian summer monsoon (ASM), where deep convection serves a unique pathway for rapid transport of surface emissions and pollutants to the stratosphere. Two global CTM configurations are examined for their representation of the ASM upper troposphere and lower stratosphere (UTLS), using airborne observations collected over south Asia. Application of the developed diagnostics to the CTMs reveals the limitations of zonally-averaged surface boundary conditions for species with sufficiently short tropospheric lifetimes, and that species whose stratospheric loss rates are dominated by photolysis have excellent agreement compared to that observed. Overall, the diagnostics demonstrate the strength of airborne observations toward improving model predictions, and highlight the utility of high-resolution climate modeling to improve the understanding of reactive transport of anthropogenic pollutants to the stratosphere.

Plain Language Summary

The chemical composition of Earth's atmosphere has important implications for the health of all its ecosystems. This study establishes an approach for evaluating the representation of chemical composition in global climate models, and demonstrates the capabilities of the approach using a set of observations collected by research aircraft. We specifically focus the evaluation on the Asian summer monsoon, a region with a known pathway for transport of chemical species from near the surface into the upper atmosphere. In doing so, we identify specific areas where focused model improvement is needed.

1 Introduction

The chemical composition of Earth's atmosphere has implications for its climate and the health of all its ecosystems. Changes in atmospheric composition, induced by changes in both natural processes and anthropogenic activities, may have impacts on surface air quality, the atmosphere's energy budget, the delay of stratospheric ozone recovery as set in motion by the Montreal Protocol, among others. As such, ensuring the accurate characterization and prediction of past, present and future atmospheric composition remains a compelling research avenue.

Chemistry-climate models (CCMs) are commonly used tools to characterize and predict atmospheric composition. This type of model often sacrifices horizontal grid spacing (typically tens to hundreds of kilometers) in favor of simulating extended time periods (years to decades) with global coverage (e.g., Danabasoglu et al., 2020). Trust in any model to accurately predict the future fundamentally hinges upon its adequate representation of the past and present. Often CCMs are evaluated with satellite products and monitoring station observations using time- (e.g., monthly) or spatially- (e.g., zonal average or prescribed regions) averaged comparisons (e.g., Gettelman et al., 2019; Bossolasco et al., 2021; Strahan et al., 2007; Froidevaux et al., 2019). Despite the known impact of regional-scale processes on atmospheric composition and climate, these processes must typically be parameterized in CCMs because their spatial (on the order of kilometers) and temporal (on the order of hours) scales are not compatible with a typical CCM's grid configuration. To evaluate and improve the representation of regional-scale processes

in CCMs, it is necessary to evaluate them for shorter time periods or for specific regions. In this configuration, a CCM is integrated as a chemistry transport model (CTM).

Airborne field campaigns for targeted regions and/or specific phenomena can provide observations to elucidate regional-scale processes affecting atmospheric composition (e.g., Pan et al., 2010, 2017; Toon et al., 2016). Airborne instruments have the capability to sample a portion of the atmosphere in unparalleled detail given their high sampling frequency. However, the high spatial and temporal resolution over a confined area fall into sharp contrast with the grid structures of CTMs, which can make their application for model evaluation difficult to reconcile. Global CTMs typically use horizontal grid spacing of tens or hundreds of kilometers, making them much coarser than airborne in situ observations which are often spaced at hundreds or thousands of meters. As such, specific diagnostic tools are needed to minimize the fundamental differences in air mass sizes represented by in situ observations and CTMs. A straightforward technique is to interpolate a flight track onto a CTM's grid and compare this with observations taken along the same flight track, but given the aforementioned disparities in air mass sizes this approach may underutilize the full capabilities of both the observations and model.

The goal of this study is to demonstrate the use of airborne in situ observations to diagnose CTM representation of deep convective transport to the UTLS and subsequent stratospheric loss processes. Specifically, we present newly-developed process-based diagnostics which use both dynamical and chemical coordinates to minimize the fundamental differences in air mass sizes represented by airborne in situ observations and CTMs. Surface boundary conditions (i.e., surface mixing ratios), dynamics, and chemistry are all considered in the diagnostic development. In doing so, we demonstrate the wealth of information contained within airborne in situ observations, and show that this approach of connecting observations and models enhances the value of each.

The specific process of the present evaluation is the Asian summer monsoon (ASM), a dominant weather system during boreal summer which has long been known for its generation of seasonal rainfall over portions of Asia (e.g., Yin, 1949). The line of research we focus on in this work concerns the air mass that is transported from the Asian boundary layer (BL) through ASM deep convection and its subsequent transport. Specifically, water vapor and tropospheric pollutants can be transported vertically through convection to reach the upper troposphere and lower stratosphere (UTLS), where they have the potential to impact global atmospheric composition and climate (e.g., Dethof et al., 1999; Fu et al., 2006; Chen et al., 2012; Fan et al., 2017). The application of chemical and transport modeling techniques to predict ASM impacts on global atmospheric composition remains an active research area (e.g., Ploeger et al., 2017; Vogel et al., 2019; Yan et al., 2019; Pan et al., 2016, 2022; Clemens et al., 2023).

The dynamical response to ASM deep convection, an anticyclone which forms in the UTLS during boreal summer (Krishnamurti & Bhalme, 1976), has been observed by satellite to show confinement of anomalous pollutant concentrations of anthropogenic signature (e.g., Park et al., 2004, 2007; Randel et al., 2010). Tropopause altitudes over the ASM are typically higher than the surrounding regions, so ASM pollutants detrained from deep convection may be subsequently transported to the stratosphere through quasi-isentropic mixing as they spiral upward anticyclonically (e.g., Pan et al., 2016; Vogel et al., 2019; Legras & Bucci, 2020). Short-lived halogenated species transported to the UTLS in this way may delay the recovery of stratospheric ozone (e.g., Bednarz et al., 2022), where the modeled impact depends on the complexity of the chemical mechanism or treatment considered (Fernandez et al., 2021). The potential for the ASM to impact atmospheric composition and climate makes it an ideal setting for the development of CTM evaluation diagnostics.

Table 1. A collection of StratoClim data used for the development of model diagnostics in this study, including the sensors or instruments that obtained them.

Instrument	Species Used	PI	Reference
AMICA	Carbon Monoxide (CO)	M. von Hobe	Kloss et al. (2021)
COLD2	Carbon Monoxide (CO)	S. Viciani	Viciani et al. (2018)
FOZAN-II	Ozone (O_3)	F. Ravegnani	Ulanovsky et al. (2001)
HAGAR	Nitrous Oxide (N_2O)	C. M. Volk	Homan et al. (2010)
WAS	Halogenated Species	J. Laube	Adcock et al. (2021)

The model evaluation and diagnostic development is broken down into three specific processes which loosely encompass the pathway for anthropogenic pollution emitted over Asia to impact UTLS composition, and thus global climate. Each analyzed process results in the development of a diagnostic, and is presented in its own subsection within Section 3. First, we use an adjusted-tropopause relative altitude coordinate to diagnose transport of polluted air masses from the Asian BL to the ASM UTLS anticyclone via deep convection (Section 3.1). Next, we diagnose the modeled mixing ratios of halogenated species as they cross the ASM tropopause and enter the stratosphere (Section 3.2). Finally, we diagnose model chemical loss rates in the stratosphere by using the mixing ratio of long-lived tracers as a vertical coordinate (Section 3.3). To demonstrate the value of the diagnostic development, we evaluate two CTMs with different grid configurations (Section 2.2) by using a set of airborne in situ observations taken over south Asia during the ASM's active period (Section 2.1).

2 Tools for Diagnostic Development

2.1 Airborne in situ observations from StratoClim 2017

Motivated by the pronounced impacts of the ASM on UTLS composition, the StratoClim airborne field campaign (http://www.stratoclim.org/; von Hobe et al., 2021; Bucci et al., 2020) was conducted during boreal summers 2016 and 2017 with bases in Kalamata, Greece and Kathmandu, Nepal, respectively. As the 2017 deployment took place over southern Asia, the region identified as the predominant source of convective uplift for the ASM UTLS anticyclone (e.g., Bergman et al., 2013; Vogel et al., 2015; Pan et al., 2016), we use only the 2017 observations throughout this paper, and henceforth refer to this deployment as "the StratoClim campaign" for simplicity. The StratoClim campaign conducted eight research flights onboard the M55 Geophysica between July 27 and August 10, 2017. The location of the experiment is shown in Figure 1 with dynamical context. The research flights primarily sampled the interior of the ASM UTLS anticyclone (e.g., Figure 1 of von Hobe et al., 2021). Here we also show the flight tracks relative to the seasonal location of the anticyclone from a geopotential height perspective (panel a) as well as in pressure (panel b) and potential temperature (panel c) space.

We use chemical observations obtained by several airborne instruments onboard the M55 Geophysica for the diagnostic development herein. The measurements are summarized in Table 1, and we direct the reader to the listed references for specifics about the instruments. In the interest of being thorough, we include a few pertinent details below.

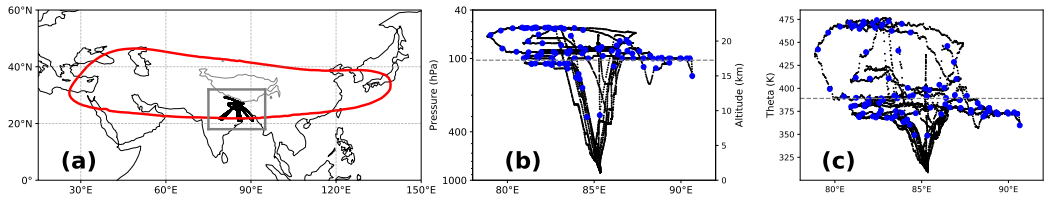

Figure 1. Setting of the StratoClim 2017 experiment with flight tracks shown in black. In panel a, the red contour shows the geopotential height contour of 16.77 km at 100 hPa (threshold taken from Bian et al., 2012) from Global Forecasting System (GFS) analysis averaged over the StratoClim measurement period, and the gray box shows the domain which the models are subset to throughout Section 3. Panels b and c show the flight tracks in vertical perspective using pressure, altitude and potential temperature vertical coordinates. Whole Air Sampler (WAS) observation points marked in blue, and dashed gray lines denote the mean tropopause during the StratoClim sampling period.

2.1.1 AMICA Carbon Monoxide

Observations of the tropospheric-sourced trace gas carbon monoxide (CO) are used to diagnose properties of convective transport. We use CO observations from the Airborne Mid-Infrared Cavity enhanced Absorption spectrometer (AMICA, Kloss et al., 2021), which was deployed for the first time during the StratoClim campaign. These data are available on 10 second intervals, are estimated to have an overall accuracy of better than 5% and a 1σ precision of $\sim$20 ppb. These data have been previously analyzed toward understanding the dynamical and transport properties of the ASM by von Hobe et al. (2021).

2.1.2 COLD2 Carbon Monoxide

We also include CO observations from the Carbon Oxide Laser Detector 2 (COLD2, Viciani et al., 2018) instrument. COLD2 observations have a higher sampling frequency, with data available on a 1 second interval. The CO mixing ratio accuracy is estimated to be 3%. The COLD2 instrument has now been deployed for two ASM-centric campaigns: both StratoClim and the Asian summer monsoon Chemical and Climate Impact Project (ACCLIP 2022, Pan et al., 2022).

2.1.3 FOZAN-II Ozone

Ozone (O_3) is commonly used as a stratospheric tracer, making it an important component of the diagnostic development herein. We use observations of ozone taken from the Fast OZone ANalyzer (FOZAN-II, Yushkov et al., 1999; Ulanovsky et al., 2001) during six of the eight StratoClim flights in 2017. FOZAN-II sampling time is 1 second, the sensitivity is about 1 ppbv, and the average accuracy is 7%.

2.1.4 HAGAR Nitrous Oxide

We use observations of nitrous oxide (N_2O) due to its long tropospheric lifetime (15,600 years, SPARC Report No. 6), making it ideal to use as a chemical vertical coordinate in the stratosphere. This was measured during StratoClim by the High Altitude Gas AnalyzeR (HAGAR, Homan et al., 2010). The measurements have a 90 second sampling interval, an average precision of $\sim$0.5% and an average accuracy of $\sim$0.6%.

2.1.5 WAS Halogenated Species

To assess the modeled chemical mechanisms, we make use of air samples collected by a Whole Air Sampler (WAS) during StratoClim, which were subsequently analyzed for a wide range of halogenated species (Adcock et al., 2021). Selected species for this study include methyl halides, (hydro)chlorofluorocarbons ((H)CFCs), with a focus on species emphasized in Adcock et al. (2021) due to their ready availability. These species are produced by both natural and anthropogenic activities, and if lofted to the stratosphere can lead to the catalytic destruction of ozone. Each StratoClim flight included a maximum of 20 WAS samples, each with sampling duration of a few minutes. The sampling was performed on a non-uniform time grid, as depicted in Figure 1 (blue dots in panels b and c). Uncertainty information from each sample is provided via Adcock et al. (2021). "Merged" datasets onto the WAS measurement time interval are used in Section 3 to account for the irregular sampling intervals for this instrument. This is done by averaging all observations that fall between a given WAS canister's open and close times.

2.2 Chemistry Transport Model Configurations

Use of the diagnostics developed herein is demonstrated using two atmosphere model components within the NCAR Community Earth System Model version 2 (CESM2, Danabasoglu et al., 2020). The first model is the Whole Atmosphere Community Climate Model version 6 (WACCM6, Gettelman et al., 2019) which uses a 0.95° latitude x 1.25° longitude grid with 110 vertical levels spanning from the surface to ∼140km (Garcia and Richter, 2019). This vertical level configuration gives WACCM a vertical grid spacing of ∼500 m in the UTLS. The second model is the recently-developed MUlti-Scale Infrastructure for Chemistry and Aerosols version 0 (MUSICAv0, Schwantes et al., 2022), which has the capability for user-customized horizontal grid refinement to improve sampling over a region of interest. For the current work, a custom MUSICA grid is developed with refinement to ∼30 km horizontal spacing over southeastern Asia and the western north Pacific (Figure S1a), while the remainder of the globe is covered by ∼1° spacing (similar to WACCM). The MUSICA grid uses 32 vertical levels spanning from the surface to ∼80km (∼3 hPa), resulting in a ∼1km vertical grid spacing in the UTLS. The vertical grid increments in WACCM and MUSICA are shown in Figure S1b. Output from the WACCM (MUSICA) simulation is available on 3- (6-) hour intervals.

Both WACCM and MUSICA utilize a specified dynamics option which nudges the temperature and zonal and meridional wind components to a chosen meteorological analysis. For this we use the Modern-Era Retrospective analysis for Research and Applications version 2 (MERRA-2, Gelaro et al., 2017). Global surface emissions are provided by the Copernicus Atmosphere Modeling System (CAMS, Granier et al., 2019). The chemistry mechanism in CESM2 includes a total of 231 species and 538 chemical reactions and is described by Emmons et al. (2020). The simulations parameterize deep convection using the Zhang-McFarlane scheme (Zhang & McFarlane, 1995). Other parameterizations are given by Gettelman et al. (2019) and are omitted here for brevity.

Advancements in computational processing and storage capabilities in recent years have enabled developments in finer grid spacing (i.e., higher resolution) and multi-scale grid capabilities in CTMs, such as MUSICA. In the present study, the MUSICA grid refinement is chosen to encompass the southern flank of the Tibetan Plateau (see Figure S1a), the primary "conduit" for ASM deep convective transport into the UTLS (e.g., Bergman et al., 2013; Honomichl & Pan, 2020; Clemens et al., 2023), with the intent to improve the representation of convective-scale processes responsible for lofting BL pollutants into the ASM UTLS. It remains unclear, however, whether improved grid point sampling necessarily improves a model's performance compared to a coarser-grid counterpart. This supports the establishment of process-based model evaluation diagnostics as a timely research area.

To illustrate the important role of the ASM in modifying UTLS composition, Figure 2 shows global map sections of selected chemical species from WACCM valid 500 m above the local model tropopause. A pronounced chemical signature of trace gases associated with the ASM UTLS anticyclone can be seen, similar to that of past observational and modeling studies (e.g., Park et al., 2007; Randel et al., 2010; Munchak & Pan, 2014; Pan et al., 2022), but now with consideration for filtering for a "bulging" tropopause structure over the ASM (Pan et al., 2016). The result indicates that species with tropospheric lifetimes in months (top row) have mixing ratios in the lowermost stratosphere that are larger over the ASM than anywhere else on Earth, underscoring the potential for short-lived halogenated species emitted over Asia to impact the composition of the stratosphere via the ASM transport mechanism discussed in Section 1. In contrast, species with much longer tropospheric lifetimes (bottom row) show similar mixing ratio enhancements over south Asia as in the tropical tropopause layer (TTL, Fueglistaler et al., 2009). These species are well-mixed throughout the troposphere, but begin to decay in the lower stratosphere as transport times grow longer and their chemical sinks grow stronger. Their

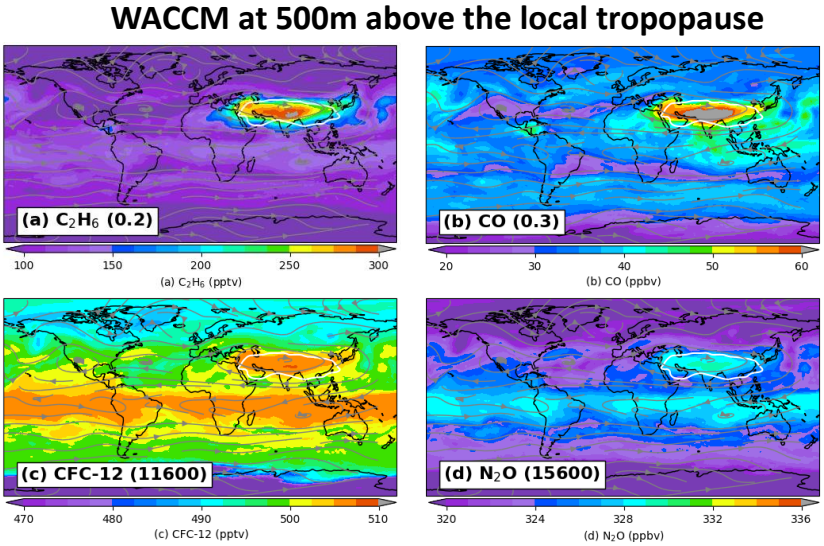

Figure 2. Plan views of WACCM model chemical species and dynamical variables in the lowermost stratosphere during the StratoClim observation period. Ethane (C_2H_6), carbon monoxide (CO), CFC-12 (CCl_2F_2) and nitrous oxide (N_2O) averaged from July 27 – August 10, 2017 and 500 m above the local WACCM tropopause are shown. White contours show WACCM tropopause altitudes greater than 16.77 km and gray lines show wind streamlines. Respective tropospheric lifetimes from SPARC Report No. 6 are given in parentheses.

highest mixing ratios in Figure 2 are simply regions where there is net upward transport across the tropopause: the TTL and the ASM.

3 Process-based Diagnostic Development and Evaluation Demonstration

3.1 Transport by Monsoon Deep Convection

Deep convection associated with the ASM is responsible for redistributing natural and anthropogenic pollutants from the BL into the UTLS (e.g., Fu et al., 2006). In this section we use high-resolution airborne data to diagnose the convective parameterization in WACCM and MUSICA (Zhang and McFarlane, 1995) by evaluating how well a tropospheric and stratospheric tracer (CO and ozone, respectively) are distributed throughout the free troposphere and UTLS compared to observations.

To examine vertical transport of CO and ozone, vertical distributions of the StratoClim observations and model results for South Asia are shown in Figure 3. Tracer mixing ratios are compared using two different vertical coordinates: adjusted tropopause-relative altitude, which expands the tropospheric layer and highlights the air mass transition across the tropopause, and potential temperature, which collapses the tropospheric layer to highlight the transition between convective-dominated and radiative-dominated ascent processes. The lapse rate tropopause (LRT) altitude from ERA5 reanalysis (Hersbach et al., 2020; Hoffmann & Spang, 2022) is interpolated to the flight tracks for observations, while the model-derived LRT is used for WACCM and MUSICA. The tropopause-relative altitude coordinate has utility for understanding the behavior of ASM convective transport relative to the tropopause, and enables adjustment for subtle differences

between model dynamics and those in the real atmosphere. This analysis is complementary to and extends that of von Hobe et al. (2021), by analyzing how models represent tracer behavior in the ASM region.

The result shows that MUSICA and WACCM have a generally good agreement with CO observations from AMICA and COLD2, mixing ratios ranging from ∼70-140 ppbv throughout the troposphere and gradually decreasing to ∼15-30 ppbv in the lower stratosphere in both observations and models (Figure 3, left panels). CO observations have a similar distribution of CO throughout the majority of free tropospheric altitudes, suggesting that convection is the dominant transport process up to ∼1-2 km below the local tropopause (∼15km altitude on average). Separate maxima in modeled CO in the lower and upper troposphere show the influence of shallow and deep convective modes of transport, respectively. In potential temperature space, the noticeable discontinuity at ∼360K clearly reveals the transition from convective-dominated to radiative-dominated ascent.

On the other hand, MUSICA and WACCM struggle to represent the observed distribution of ozone, with a high bias spanning between the free troposphere and lower stratosphere (Figure 3, right panels). This is not particularly surprising, as WACCM and MUSICA ozone has been noted to have a high bias in previous work when compared to observations (Froidevaux et al., 2019; Dubé et al., 2022; Tang et al., 2023). Ozone mixing ratios observed by FOZAN-II are further supported by ozonesonde observations over Nepal during StratoClim, which show ∼30-50 ppbv ozone throughout the free troposphere (Brunamonti et al., 2018). We have performed several sensitivity experiments to elucidate the cause of the model high bias, including testing for sensitivity to chemistry of very short lived (VSL) species using the model configuration of Villamayor et al. (2023), and to adjusting the model's lightning parameterization to generate less NOx (an ozone precursor). The results of these sensitivity runs on model ozone mixing ratios shown in Figure S3. Although these experiments reduce the model's ozone, they do not explain a sufficiently large bias to close the gap with the observations. More generally, these sensitivity experiments demonstrate another application of the dynamical coordinate diagnostic, highlighting its utility in interrogating modeled representations of tracer mixing ratios.

A critical component to the analysis presented in Figure 3 is that model distributions are computed from broader spatial and temporal boundaries compared to the StratoClim flight tracks. Specifically, the model distributions are an average of all grid points between 75-95°E longitude, 18-32°N latitude (the gray box printed on Figure 1a), and at every 3- or 6-hour interval between July 27 – August 10, 2017. Instead of comparing each observation to a much larger model grid cell through interpolation (we demonstrate this common technique in Figure S2 for context), our technique allows a comparison of the general behavior of ASM transport throughout the monsoon's active phase. We acknowledge that flight campaigns often bias their sampling to specific phenomenon (e.g., convective complexes, wildfire plumes, etc.) which could complicate the interpretation of this evaluation, however most StratoClim flights were designed to survey the large-scale characteristics of the ASM UTLS, which supports the compatibility of this evaluation technique (Bucci et al., 2020).

To demonstrate an additional use of the dynamical vertical coordinates used in this analysis, we compare distributions of the tropospheric tracer CO in Figure 4 at key vertical layers identified from analyzing Figure 3. This allows for a more quantitative evaluation of the models against the observations, as well as a quantitative comparison of the WACCM and MUSICA grid configurations following the discussion in Section 2.2. The general similarity between observations and models at each of the selected layers corroborates with the qualitative agreement noted in Figure 3. Mean values from the distributions are collected in Table 2.

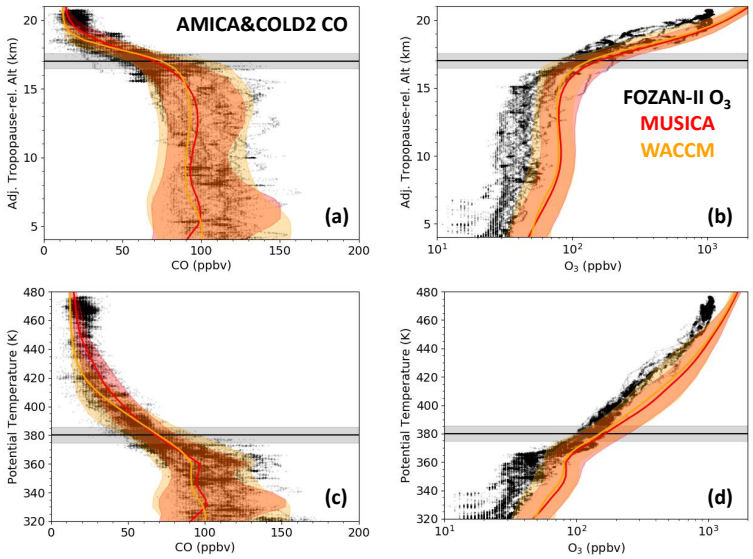

Figure 3. Vertical profile distributions of modeled and observed (left) CO and (right) ozone mixing ratio vertical profiles from models and StratoClim observations. The top panels are plotted in tropopause-relative altitude space while the bottom panels are plotted in potential temperature space. Black dots show StratoClim observations, and MUSICA (WACCM) results are plotted in red (orange), where solid lines show the mean and shaded regions show the 5th to 95th percentile range. The tropopause is denoted by the solid black line with its standard deviation marked by gray shading. Y-axes in the top panels are "adjusted" by the mean tropopause value for ease of comprehension. Model output is restricted to 75-95 E, 18-32 N (gray box in Figure 1a) from July 27 - August 10, 2017.

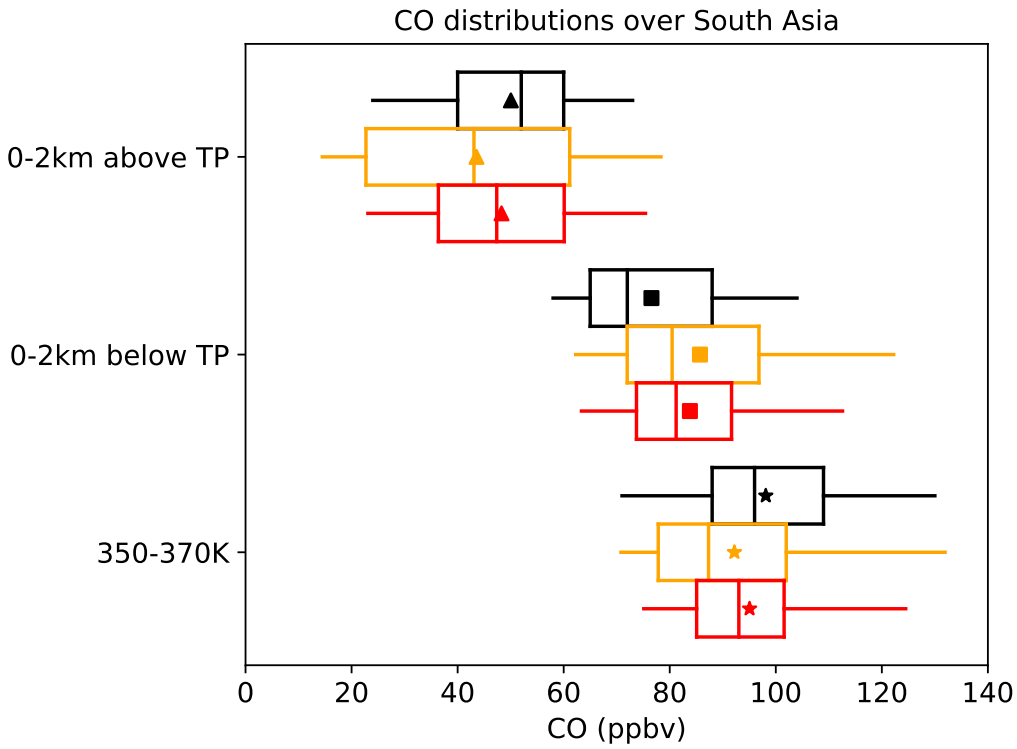

Figure 4. Box and whisker plots for CO mixing ratios within selected vertical ranges, with observations from AMICA and COLD2 in black, WACCM in orange, and MUSICA in red. "Boxes" span from the 25th to 75th percentiles, "whiskers" span from the 5th to 95th percentiles, and the vertical lines in the "boxes" represent the median. Mean mixing ratios are plotted as triangles (squares) for 0 to 2km above (below) the local tropopause (abbreviated as "TP" on the y axis), and as stars for 350 K to 370 K potential temperature.

There is no obvious advantage demonstrated by the MUSICA simulation with refined horizontal grid spacing at the level of primary convective outflow (stars in Figure 4 and Table 2). This may be because convection must still be parameterized with the MUSICA grid configuration. Interestingly however, CO mixing ratios distributions in the lowermost stratosphere (triangles in Figure 4 and Table 2) suggest a low bias compared to observations. Although the present work does not pursue model improvements to address these discrepancies, the examples provided here are evidence for how the diagnostics using these dynamical coordinates may identify specific areas for targeted model interrogation and development.

3.2 Transport Across the ASM Tropopause

Polluted air masses lofted by deep convection may be deposited higher than the level of zero radiative heating (LZRH, ∼360K in the tropics, Ploeger et al., 2010), above which air masses preferentially undergo comparatively slow ascent. Polluted air masses which cross the ASM tropopause, either vertically or through quasi-isentropic transport to the surrounding lower-tropopause regions (e.g., Pan et al., 2016; Vogel et al., 2019), may thus have the potential to impact global composition and climate. Modeling the appropriate mixing ratios of pollutants at the ASM tropopause is thus an important com-

Table 2. Mean CO mixing ratios (ppbv) in each selected vertical range shown in Figure 4.

Layer Symbol	0-2 km above LRT Triangle	0-2 km above LRT Square	350-370 K θ Star
AMICA/COLD2	43.2	69.4	98.1
WACCM	43.6	85.7	92.2
MUSICA	48.3	83.8	95.1

ponent of representing the ASM's impacts. This section diagnoses the model representation of halogenated species and N_2O mixing ratios in the ASM tropopause layer.

Selected halogenated species and N_2O from WACCM, MUSICA, and StratoClim airborne observations from the WAS and HAGAR instruments (respectively) are shown in Figure 5. As in Section 3.1, we use an adjusted tropopause-relative coordinate to adjust for dynamical differences in models compared to that in the real atmosphere. The result shows that the models have qualitatively good representation of the four selected species at the ASM tropopause. For species with tropospheric lifetimes longer than one year, tropospheric mixing ratios are nearly constant with altitude given this is long compared to typical overturning of the troposphere (typically 2-3 weeks). Thus, their mixing ratio accuracy at the tropopause is mainly controlled by the model's lower boundary condition used to prescribe surface mixing ratios. We note there is a slight high bias in modeled mixing ratios found ∼2-3 km above the local tropopause in all panels of Figure 5. This suggests an error in the behavior of model dynamics in the lower stratosphere, either through vertical motion or mixing from the surrounding regions. The model representation of the lower stratosphere will be addressed in more detail in Section 3.3.

Although the modeled species tropopause mixing ratios depicted in Figure 5 are qualitatively encouraging, we wish to establish a quantitative diagnostic to characterize the error in modeled stratospheric entry mixing ratios, to easily identify species which are simulated (in)adequately. For this, we calculate the mean observed and modeled mixing ratios near the local tropopause (we choose within 1 km above and below; see the gray regions in Figure 5) and compare their difference against the "observational range of variability", to characterize biases which are large compared to the mixing ratio range throughout the ASM UTLS. Put mathematically:

$$Stratosphere\ Entry\ Error = \frac{q_{t,m} - q_{t,o}}{\Delta q_o} * 100\% \quad (1)$$

where q is the mixing of a given specie, the subscript t indicates the mean mixing ratio within 1 km of the local tropopause (as shown in Figure 5) during the StratoClim period, and the subscript m (o) indicates modeled (observed). Δq_0 is the difference between the maximum and minimum observed mixing ratio in the entire StratoClim dataset (i.e., the "observational range of variability"). The results are shown in Figure 6.

The calculation of error statistics, as done in Figure 6, provides a conceptual framework for identifying model skill in species representation, concisely highlighting areas where focused model development is needed. It also allows for different model configurations to be compared relative to one another. In the current approach, we see mostly superficial differences between WACCM and MUSICA in their stratospheric entry mixing ratio performance, likely a consequence of the same emissions database used in the simulations. Most species have stratospheric entry mixing ratio errors which are less than 10%, which we consider to be small given they could be easily explained by a combination of measurement and model uncertainties as well as the intentional sampling differ-

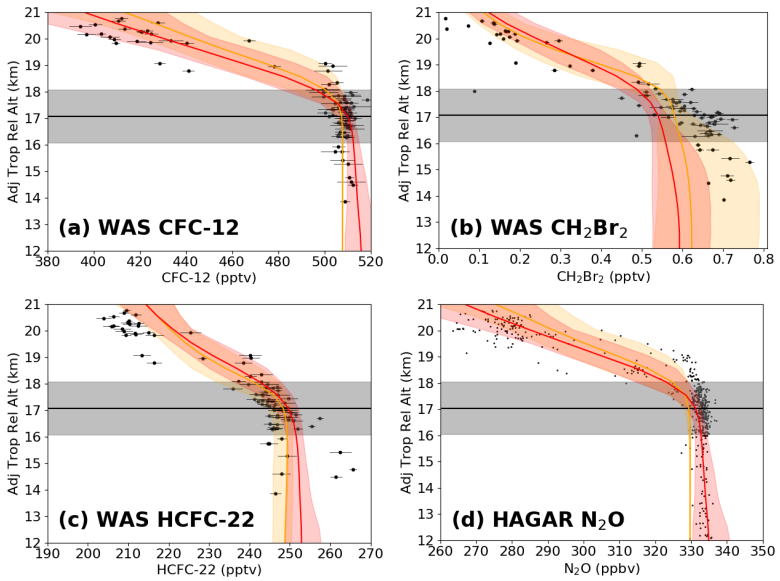

Figure 5. Modeled and observed vertical profiles of selected chemical species plotted in adjusted tropopause-relative altitude space. Black dots show observations with uncertainty plotted in thin horizontal lines. The red (orange) line shows the mean profile from the MUSICA (WACCM) simulation between 75-95E and 18-32N (the small gray box in Figure 1) from July 27 - August 10, 2017, with the corresponding shading spanning the 5th to 95th percentiles. The mean tropopause is shown as a black line, with the range of 1 km below and above it (used for calculation of the "stratospheric entry value") shaded in gray. As in Figure 3, y-axes are "adjusted" to the mean tropopause altitude for ease of comprehension.

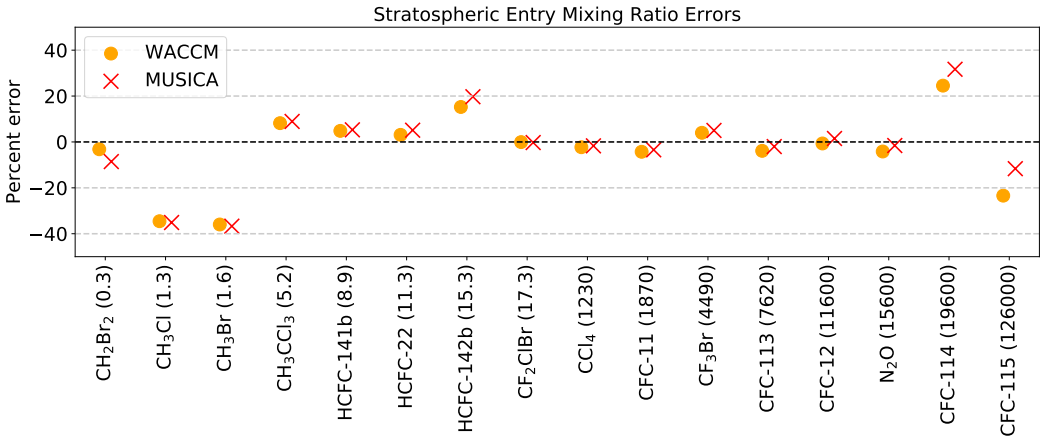

Figure 6. A scatterplot of model stratospheric entry errors for selected species. Species are sorted by their tropospheric lifetimes (SPARC Report No. 6) which are printed in parentheses in units of years.

ences we use to avoid space-time interpolation. However, this diagnostic identifies methyl chloride (CH_3Cl), methyl bromide (CH_3Br), CFC-114, and CFC-115 as species with larger errors which may have other contributing factors. Methyl chloride and bromide are of particular interest because although their tropospheric lifetimes are on the order of one year, their stratospheric lifetimes are on the order of decades (SPARC Report No. 6, Ko et al., 2013). Since these species will persist in the stratosphere for decades if they can penetrate the tropopause, and because of their impacts on stratospheric ozone chemistry (e.g., Bednarz et al., 2022), their mixing ratios in the ASM UTLS are especially important to properly represent.

To demonstrate the use of the stratospheric entry mixing ratio error calculation (Equation 1; Figure 6) in diagnosing model shortcomings, Figure 7 shows the methyl halides plotted in chemical vertical coordinate space. Both CO and CFC-12 are used as chemical coordinates to expand the tropospheric and stratospheric layers, respectively. The noticeable offsets between observed mixing ratios (black) and those from the models (red and orange) corroborate with their large errors (Figure 6). With the exception of dibromomethane (CH_2Br_2) which has the shortest tropospheric lifetime in this study, all the species analyzed in Figure 6 have mixing ratios prescribed at the model surface by using zonally-averaged mole fraction boundary conditions. Species with sufficiently long lifetimes relative to tropospheric overturning are expected to have nearly-uniform mixing ratios throughout the troposphere, as demonstrated by WACCM in Figure 2. However, for species with shorter tropospheric lifetimes such as methyl chloride and methyl bromide, this lower boundary condition may obscure important regional emissions sources, such as those from Asia, and lead to an underestimation of their composition and climate impact potentials.

The hypothesis that zonally-averaged mole fraction surface boundary conditions causes errors for methyl chloride and bromide at the stratospheric entry point can be further investigated by comparing WACCM and MUSICA results with observations outside the ASM region. For this we include in Figure 7 observations from the Studies of Emissions and Atmospheric Composition, Clouds and Climate Coupling by Regional Surveys (SEAC^{4}RS) campaign, which took place over North America during boreal summer 2013 (Toon et al., 2016), as gray dots. SEAC^{4}RS observations align nicely with the 2017 WACCM and MUSICA simulations subset to the ASM region (gray box in Figure

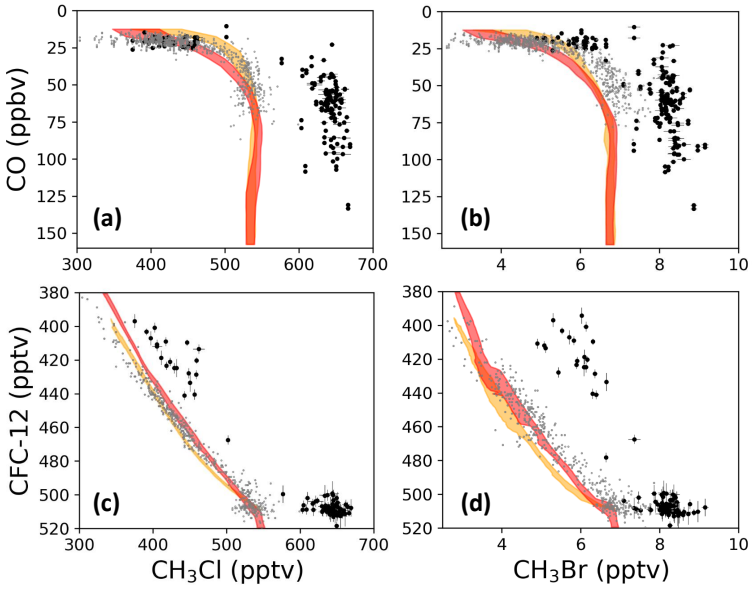

Figure 7. Vertical profiles of (left) methyl chloride and (right) methyl bromide in chemical coordinate space using (top) CO and (bottom) CFC-12 as the vertical coordinates. WACCM (MUSICA) mixing ratios from the 5th to 95th percentiles are shown in orange (red). Black dots show airborne observations from StratoClim (2017) with uncertainty bars, and gray dots show airborne observations from SEAC^{4}RS 2013 (Toon et al., 2016) taken over North America. To ensure compatibility between the campaigns, we adjust the CFC-12 mixing ratios from SEAC^{4}RS according to the long-term trend between 2013 and 2017, using observations from the NOAA/GML halocarbons program (Dutton et al., 2023).

1), indicating that model mixing ratios reflect the ASM's surroundings rather than the ASM environment itself. This supports our assertion that the prescribed zonally-averaged boundary condition assumption breaks down for species with tropospheric lifetimes less than a few years. More broadly, this analysis highlights the value of the stratospheric entry diagnostic at identifying model shortcomings and providing a pathway for focused improvements.

3.3 Chemical Loss in the Lower Stratosphere

The two previous sub-sections focus on transport of Asian pollution into the UT via convective transport (Section 3.1), and subsequent entry to the stratosphere (Section 3.2). In this sub-section we diagnose the model representation of chemical loss processes in the lower stratosphere, using a "chemical vertical coordinate." The relatively coarse vertical grid spacing in MUSICA which degrades further in the lower stratosphere (Figure S1b) leads us to focus this evaluation on the WACCM simulation only. Furthermore, due to the aforementioned issues with methyl halide species (Figures 6 and 7) and the inappropriateness of a linear fit for dibromomethane (CH_2Br_2; not shown), these species are excluded from this chemical loss analysis.

Following the approach of Avallone and Prather (1997), a collection of tracer relationships for halogenated species and N_2O are plotted in Figure 8 with CFC-12 mixing ratio used as the vertical coordinate for both WACCM and StratoClim observations. Although the full range of variability is plotted, we focus on the cluster of stratospheric observations between 394-442 pptv of CFC-12, to ensure the tracer relationships are con-

sistent with the observations. For this range of mixing ratios, linear "best fit" lines are calculated for both observations (black lines) and WACCM (brown lines). Measurement uncertainty (from Adcock et al., 2021) is accounted for by assigning weights to each point for the linear fitting, equal to the inverse of the sum of both the squared mixing ratio uncertainties. Furthermore, we discard two WAS data points (one for CCl_4 and another for CFC-114) which are clear outliers, and by inspection disrupt the appropriateness of the linear fit (not shown).

From the foundational arguments of Plumb and Ko (1992) on tracer relationships: "the curve becomes linear in any region if the net upward fluxes of two species through the rapid exchange surfaces in that region are in constant ratio." Indeed, the modeled and observed relationships exhibit linear behavior in the lower stratosphere (Figure 8), suggesting the species lifetimes are long in this layer compared to the timescales of net upward flux. From a conceptual standpoint, the chemical mechanism in WACCM has excellent representation of this behavior. In contrast, many relationships in Figure 8 exhibit non-linear behavior closer to the tropopause (∼500 pptv of CFC-12; see Figure 5), a consequence of the large lifetime disparity between the species on each axis. Often in these cases, the observations (gray dots) are considerably less compact than both WACCM (light orange dots) and their deeper stratospheric counterparts (black dots).

To quantify the ability of WACCM to represent the observed tracer relationships, a diagnostic is developed that is based on the modeled and observed chemical loss rate (i.e. slopes of the linear fitting). Often the WACCM loss rates are similar to those observed, but are "offset" in absolute mixing ratio (Figure 8). To calculate the loss rate and mixing ratio offset errors, we employ similar formulas as Equation 1 for the stratospheric entry mixing ratio errors:

$$Loss\ Rate\ Error = \frac{m_{ls,W} - q_{ls,o}}{\Delta m_{ls,0}} * 100\% \tag{2}$$

$$Mixing\ Ratio\ Offset\ Error = \frac{q_{ls,W} - q_{ls,o}}{\Delta q_{ls,o}} * 100\% \tag{3}$$

In Equations 2 and 3, the subscript ls denotes the selected lower stratospheric range, m indicates the slope of the linear relationships, q indicates the x-axis tracer mixing ratio at the midpoint of the lower stratospheric range considered (i.e., 418 pptv of CFC-12), and subscripts W and o indicate modeled by WACCM and observed, respectively. The diagnostics in Equations 2 and 3 enable a quantitative evaluation of WACCM's performance at representing the observed tracer relationships, separating the model representation of lower stratospheric dynamics and chemistry from offsets in the absolute mixing ratios found there.

To demonstrate the application of the loss rate and mixing ratio error diagnostics defined here, Figure 9 shows calculated results for the choice of two chemical vertical coordinates and two model domain selections. The selected vertical coordinates are CFC-12 (Figure 8) and N_2O (Figure S4, for which a range of 265-292 ppbv is chosen for the lower stratosphere). The two domain selections are that shown in the gray box in Figure 1 (75-95E, 18-32N; denoted "small"), which is used throughout Sections 3.1 and 3.2, and a larger domain which approximately represents the ASM UTLS anticyclone (30-130E, 18-40N; denoted "large").

The mixing ratio offset diagnostic (Equation 3) shows errors for all species which are less than 20% (Figure 9a), which is conceptually consistent with the stratospheric entry diagnostic presented in Section 3.2 (Figure 6). Indeed, a species with an accurate mixing ratio at the tropopause is predisposed to an accurate mixing ratio in the lower stratosphere. While the loss rate diagnostic (Equation 2; Figure 9b) also shows errors of less than 20% for most relationships, it identifies CFC-114 and CFC-115 as species

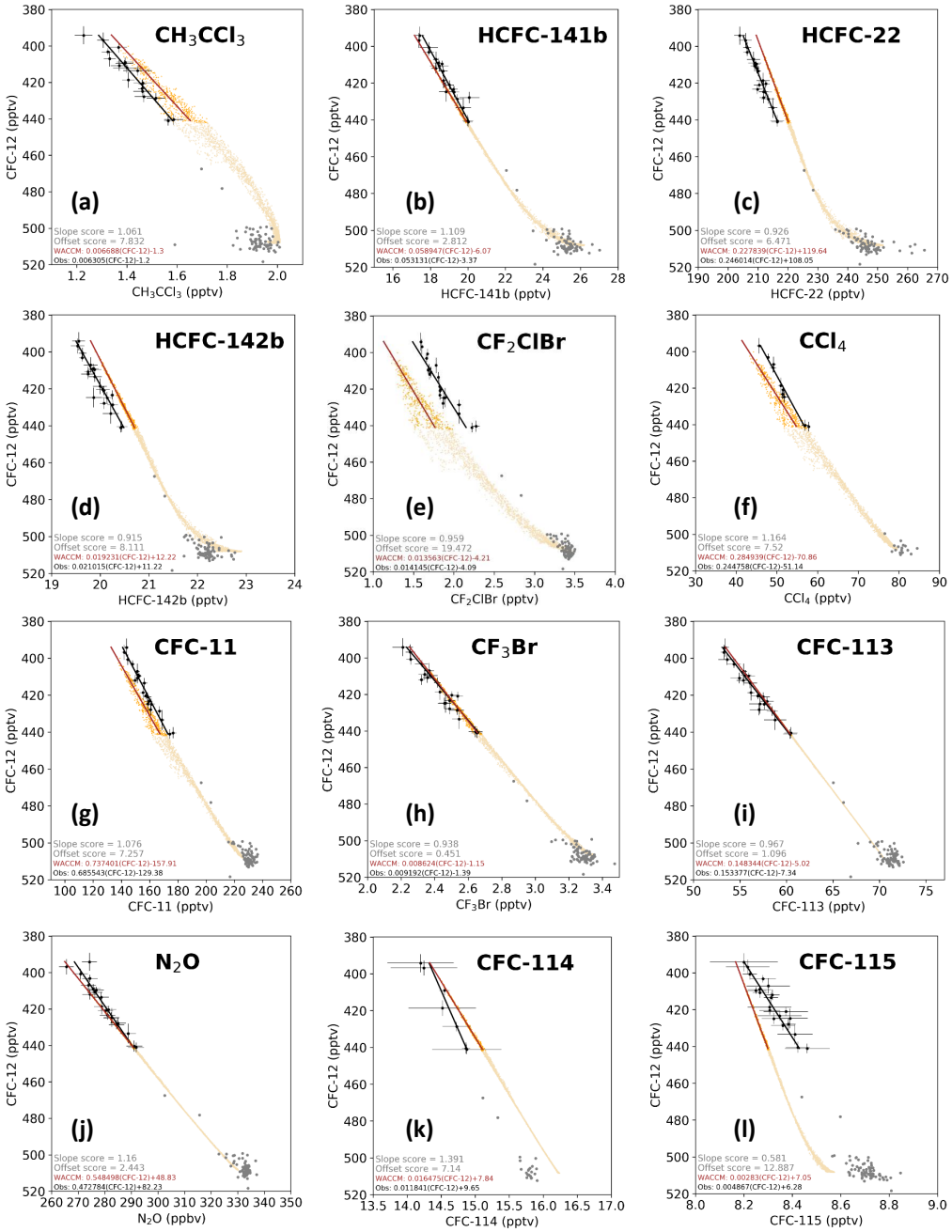

Figure 8. Various halocarbon and N_2O profiles in CFC-12 chemical vertical coordinate space. Black dots show StratoClim observations in the lower stratosphere (394 pptv < CFC-12 < 442 pptv), with thin lines marking observational uncertainty. Thick black lines mark observational best-fits using a weighted linear regression. WACCM is shown in orange, with brown lines marking the linear model best-fit in the lower stratosphere. WACCM is subset between 78-92E, 18-32N (the small gray box in Figure 1), from July 27 - August 10, 2017, to 50-200 hPa to focus on the UTLS, and to every 50th point for visual clarity. Light orange and gray dots show model and observation points (respectively) near and below the tropopause, which are not used for the linear fitting.

with considerable deviations from the observed loss rates in chemical coordinate space. These deviations in loss rate, coupled with their poor stratospheric entry mixing ratio representation (Figure 6), are evidence that WACCM does not properly represent them. For both CFC-114 and CFC-115, loss by O^1D is an important process in comparison to loss by photolysis (from SPARC Report No. 6, 2013), which we highlight using asterisks in the Figure 9 labeling. With this in mind, we find it reasonable to hypothesize that the model ozone high bias noted in Section 3.1 (Figure 3) contributes to the errors in these relationships, as ozone is the main source of O^1D in the lower stratosphere. A subsequent model experiment was performed with a longer spin-up to test for sensitivity in CFC-114 and CFC-115 given their relatively long stratospheric lifetimes, which did not yield improvements to this relationship (not shown).

We clarify again that it is not our objective to make corrections to the chemical mechanisms in the present work, only to show the utility of this diagnostic framework for identifying areas for focused model improvement. Investigating the shortcomings of these relationships are the subject of ongoing work, and may require the use of idealized chemical modeling to understand the complex mechanisms contributing to these relationships.

With the use of the stratospheric mixing ratio offset and chemical loss rate diagnostics in this subsection, we demonstrate that WACCM chemistry overall performs well at representing the chemical relationships observed during StratoClim. As with prior analyses, this diagnostic minimizes the impact of fundamental air mass size disparities between observed and modeled air masses. Both diagnostics show a general consistency between the two choices of chemical vertical coordinate as well as the two choices of domain. The consistency between the two domain choices suggests that the ASM anticyclone has a composition signature in the lower stratosphere that is fairly consistent throughout; despite the StratoClim campaign spanning only a modest portion of the ASM UTLS anticyclone.

4 Conclusions and Outlook

In this study we design a set of process-based diagnostics using airborne in situ chemical tracer measurements to evaluate the representation of UTLS composition under the influence of ASM dynamics and transport. The diagnostics are:

1. The use of tropopause-relative altitude and potential temperature vertical coordinates to evaluate distributions of tropospheric and stratospheric tracers (Section 3.1). These coordinates adjust for dynamical differences between models and the real atmosphere, and allow for the properties of modeled and observed convection to be diagnosed.
2. The use of a tropopause-relative altitude vertical coordinate to evaluate stratospheric entry mixing ratios of chemical species (Section 3.2). For species with tropospheric lifetimes which are long compared to typical tropospheric overturning time scales, this diagnoses the representation of the mixing ratio boundary condition used at the model surface.
3. The use of long-lived tracers as a vertical coordinate to diagnose chemical loss processes in the lower stratosphere (Section 3.3). The application of this to a wide range of species identifies those which may have issues in their chemical treatment by the model.

We demonstrate the application of the above diagnostics in two global climate models run in CTM configuration (WACCM and MUSICA) using airborne in situ observations from the ASM region (StratoClim 2017). The exercise leads to the following conclusions about the representation of ASM composition by WACCM and MUSICA:

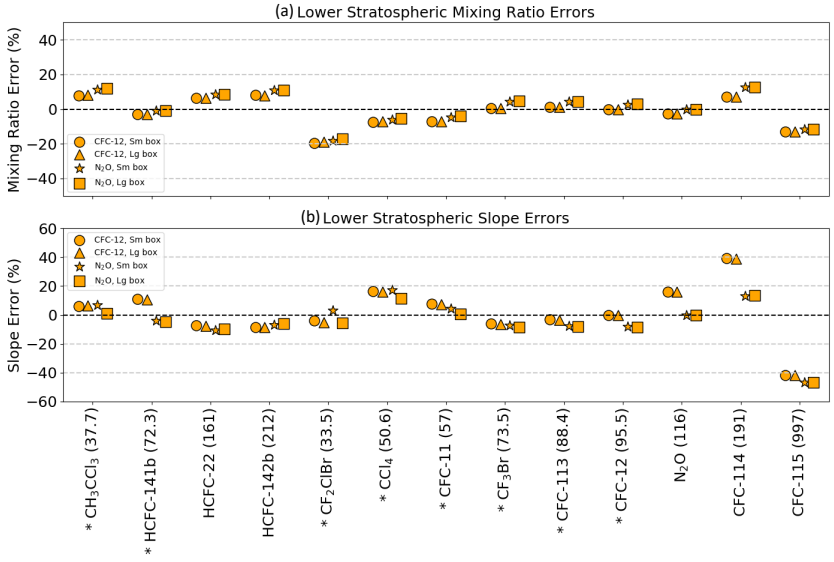

Figure 9. Scatterplots showing (a) mixing ratio errors and (b) loss rate errors between observations and models in the lower stratosphere. Symbols show calculations using CFC-12 and N_2O as the choice of chemical vertical coordinate, as well as two model domain choices (see text for details). Species are organized in the same order as Figure 6, but with their stratospheric lifetimes in years (SPARC Report No. 6) now printed in parentheses instead. Asterisks mark species whose loss is primarily controlled by photolysis.

- The level of ASM deep convective outflow (∼15km; ∼360K) and distribution of CO observed during StratoClim are generally well-represented by WACCM and MUSICA. Both models show similar CO mixing ratios in key altitude ranges, despite differences in their horizontal and vertical grid increments. However, there is a high model bias in ozone throughout the free troposphere.
- Observed tracer mixing ratios at the ASM tropopause are generally consistent with those in WACCM and MUSICA. For species with relatively short tropospheric lifetimes (less than a couple of years), representing mole fraction boundary conditions with a zonal average obscures important regional emissions sources which may lead to large model biases, as shown to be the case for methyl chloride and methyl bromide.
- The use of long-lived chemical vertical coordinates reveals that WACCM represents the compact nature of chemical relationships observed in the lower stratosphere. Species whose stratospheric loss rates are dominated by photolysis have particularly good agreement in their chemical loss rates compared to observations, while the high model ozone bias may negatively impact the representation of loss for other species.

Climate prediction is often conducted on spatial scales of hundreds of kilometers and temporal scales of decades, but accurate prediction at these scales requires accurate representation of embedded smaller-scale processes which are captured by the high spatial and temporal sampling of airborne observations. The diagnostic development and the resulting evaluation of NCAR CESM configurations herein thus highlights the irreplaceable value of airborne observations toward improving Earth system modeling capabilities. Moreover, the diagnostics are designed to minimize the fundamental differ-

ences in air mass sizes represented by models and observations, as compared to a typical method of space-time interpolation.

The establishment of this diagnostic framework may help realize the benefits, and even shortcomings, of ongoing CTM developments. Future work will examine the performance of modeling capabilities at representing a recent set of ASM airborne observations taken during the ACCLIP 2022 campaign (Pan et al., 2022). We note that although these diagnostics are designed specifically with an ASM UTLS focus, we expect them to be appropriate for other regions of the globe to evaluate their respective transport regimes.

5 Open Research

The Community Earth System Model (CESM) is an open-source community model available from http://www.cesm.ucar.edu/. The Whole Atmosphere Community Climate Model (WACCM) is described by https://www2.acom.ucar.edu/gcm/waccm, and the Multi-scale Infrastructure for Chemistry and Aerosols (MUSICA) is described by https://wiki.ucar.edu/display/MUSICA/MUSICA+Home. StratoClim data will be accessible via the HALO database at https://halo-db.pa.op.dlr.de/mission/101. Until this time, it can be provided by request from the respective instrument PIs (see Table 1). SEAC^{4}RS observations are available from https://www-air.larc.nasa.gov/cgi-bin/ArcView/seac4rs. ERA5 reanalysis (doi: 10.5065/P8GT-0R61) is available from the NCAR CISL Research Data Archive.

Acknowledgments

The National Center for Atmospheric Research (NCAR) is supported by the National Science Foundation (NSF). W.P.S. was supported under grant NSF AGS-1853929. K.E.A. was funded by the UK Natural Environment Research Council through the EnvEast Doctoral Training Partnership (grant number NE/L002582/1). We acknowledge high-performance computing support from Cheyenne (https://doi.org/10.5065/D6RX99HX) provided by NCAR's Computational and Information Systems Laboratory (CISL), sponsored by the NSF. Airborne measurements were made possible by European Community's Seventh Framework Programme (FP7/2007–2013), grant agreement 603557—Project STRATOCLIM. We acknowledge support from the Geophysica aircraft team, the StratoClim science team and the NCAR multi-scale modeling community, as well as helpful comments from M. Barth, W. Randel and E. Weatherhead.

References

Adcock, K. E., Fraser, P. J., Hall, B. D., Langenfelds, R. L., Lee, G., Montzka, S. A., ... others (2021). Aircraft-based observations of ozone-depleting substances in the upper troposphere and lower stratosphere in and above the asian summer monsoon. *Journal of Geophysical Research: Atmospheres*, *126*(1), e2020JD033137.

Avallone, L. M., & Prather, M. J. (1997). Tracer-tracer correlations: Three-dimensional model simulations and comparisons to observations. *Journal of Geophysical Research: Atmospheres*, *102*(D15), 19233–19246.

Bednarz, E. M., Hossaini, R., Chipperfield, M. P., Abraham, N. L., & Braesicke, P. (2022). Atmospheric impacts of chlorinated very short-lived substances over the recent past–part 1: Stratospheric chlorine budget and the role of transport. *Atmospheric Chemistry and Physics*, *22*(16), 10657–10676.

Bergman, J. W., Fierli, F., Jensen, E. J., Honomichl, S., & Pan, L. L. (2013). Boundary layer sources for the asian anticyclone: Regional contributions to a vertical conduit. *Journal of Geophysical Research: Atmospheres*, *118*(6),

2560–2575.

Bian, J., Pan, L. L., Paulik, L., Vömel, H., Chen, H., & Lu, D. (2012). In situ water vapor and ozone measurements in lhasa and kunming during the asian summer monsoon. *Geophysical Research Letters*, *39*(19).

Bossolasco, A., Jegou, F., Sellitto, P., Berthet, G., Kloss, C., & Legras, B. (2021). Global modeling studies of composition and decadal trends of the asian tropopause aerosol layer. *Atmospheric Chemistry and Physics*, *21*(4), 2745–2764.

Brunamonti, S., Jorge, T., Oelsner, P., Hanumanthu, S., Singh, B. B., Kumar, K. R., ... others (2018). Balloon-borne measurements of temperature, water vapor, ozone and aerosol backscatter on the southern slopes of the himalayas during stratoclim 2016–2017. *Atmospheric Chemistry and Physics*, *18*(21), 15937–15957.

Bucci, S., Legras, B., Sellitto, P., d'Amato, F., Viciani, S., Montori, A., ... others (2020). Deep-convective influence on the upper troposphere–lower stratosphere composition in the asian monsoon anticyclone region: 2017 stratoclim campaign results. *Atmospheric Chemistry and Physics*, *20*(20), 12193–12210.

Chen, B., Xu, X., Yang, S., & Zhao, T. (2012). Climatological perspectives of air transport from atmospheric boundary layer to tropopause layer over asian monsoon regions during boreal summer inferred from lagrangian approach. *Atmospheric Chemistry and Physics*, *12*(13), 5827–5839.

Clemens, J., Vogel, B., Hoffmann, L., Griessbach, S., Thomas, N., Fadnavis, S., ... Ploeger, F. (2023). Identification of source regions of the asian tropopause aerosol layer on the indian subcontinent in august 2016. *EGUsphere*, *2023*, 1–39.

Danabasoglu, G., Lamarque, J.-F., Bacmeister, J., Bailey, D., DuVivier, A., Edwards, J., ... others (2020). The community earth system model version 2 (cesm2). *Journal of Advances in Modeling Earth Systems*, *12*(2), e2019MS001916.

Dethof, A., O'neill, A., Slingo, J., & Smit, H. (1999). A mechanism for moistening the lower stratosphere involving the asian summer monsoon. *Quarterly Journal of the Royal Meteorological Society*, *125*(556), 1079–1106.

Dubé, K., Randel, W., Bourassa, A., & Degenstein, D. (2022). Tropopause-level nox in the asian summer monsoon. *Geophysical Research Letters*, *49*(18), e2022GL099848.

Dutton, G. S., Hall, B. D., Montzka, S. A., & Nance, J. D. (2023). Combined atmospheric chlorofluorocarbon-12 dry air mole fractions from the noaa gml halocarbons sampling network, 1977-2023. *https://doi.org/10.15138/PJ63-H440*.

Emmons, L., Schwantes, R. H., Orlando, J. J., Tyndall, G., Kinnison, D., & Lamarque, J.-F. e. a. (2020). The chemistry mechanism in the community earth system model version 2 (cesm2). *Journal of Advances in Modeling Earth Systems*.

Fan, Q., Bian, J., & Pan, L. L. (2017). Stratospheric entry point for upper-tropospheric air within the asian summer monsoon anticyclone. *Science China Earth Sciences*, *60*, 1685–1693.

Fernandez, R. P., Barrera, J. A., López-Noreña, A. I., Kinnison, D. E., Nicely, J., Salawitch, R. J., ... others (2021). Intercomparison between surrogate, explicit, and full treatments of vsl bromine chemistry within the cam-chem chemistry-climate model. *Geophysical Research Letters*, *48*(4), e2020GL091125.

Froidevaux, L., Kinnison, D. E., Wang, R., Anderson, J., & Fuller, R. A. (2019). Evaluation of cesm1 (waccm) free-running and specified dynamics atmospheric composition simulations using global multispecies satellite data records. *Atmospheric Chemistry and Physics*, *19*(7), 4783–4821.

Fu, R., Hu, Y., Wright, J. S., Jiang, J. H., Dickinson, R. E., Chen, M., ... Wu, D. L. (2006). Short circuit of water vapor and polluted air to the global stratosphere by convective transport over the tibetan plateau. *Proceedings of the National Academy of Sciences*, *103*(15), 5664–5669.

Fueglistaler, S., Dessler, A., Dunkerton, T., Folkins, I., Fu, Q., & Mote, P. W. (2009). Tropical tropopause layer. *Reviews of Geophysics*, *47*(1).

Gelaro, R., McCarty, W., Suárez, M. J., Todling, R., Molod, A., Takacs, L., ... others (2017). The modern-era retrospective analysis for research and applications, version 2 (merra-2). *Journal of climate*, *30*(14), 5419–5454.

Gettelman, A., Mills, M., Kinnison, D., Garcia, R., Smith, A., Marsh, D., ... others (2019). The whole atmosphere community climate model version 6 (waccm6). *Journal of Geophysical Research: Atmospheres*, *124*(23), 12380–12403.

Granier, C., Darras, S., Denier van Der Gon, H., Doubalova, J., Elguindi, N., Galle, B., ... others (2019). The copernicus atmosphere monitoring service global and regional emissions. *Reading, United Kingdom: Copernicus Atmosphere Monitoring Service. https://doi.org/10.24380/d0bn-kx16*.

Hersbach, H., Bell, B., Berrisford, P., Hirahara, S., Horányi, A., Muñoz-Sabater, J., ... others (2020). The era5 global reanalysis. *Quarterly Journal of the Royal Meteorological Society*, *146*(730), 1999–2049.

Hoffmann, L., & Spang, R. (2022). An assessment of tropopause characteristics of the era5 and era-interim meteorological reanalyses. *Atmospheric Chemistry and Physics*, *22*(6), 4019–4046.

Homan, C., Volk, C., Kuhn, A., Werner, A., Baehr, J., Viciani, S., ... Ravegnani, F. (2010). Tracer measurements in the tropical tropopause layer during the amma/scout-o3 aircraft campaign. *Atmospheric Chemistry and Physics*, *10*(8), 3615–3627.

Honomichl, S. B., & Pan, L. L. (2020). Transport from the asian summer monsoon anticyclone over the western pacific. *Journal of Geophysical Research: Atmospheres*, *125*(13), e2019JD032094.

Kloss, C., Tan, V., Leen, J. B., Madsen, G. L., Gardner, A., Du, X., ... others (2021). Airborne mid-infrared cavity enhanced absorption spectrometer (amica). *Atmospheric Measurement Techniques*, *14*(8), 5271–5297.

Ko, M. K., Newman, P. A., Reimann, S., Strahan, S. E., Atlas, E. L., Burkholder, J. B., ... others (2013). Recommended values for steady-state atmospheric lifetimes and their uncertainties. *SPARC Report on the Lifetimes of Stratospheric Ozone-Depleting Substances, Their Replacements, and Related Species*.

Krishnamurti, T. N., & Bhalme, H. (1976). Oscillations of a monsoon system. part i. observational aspects. *Journal of Atmospheric Sciences*, *33*(10), 1937–1954.

Legras, B., & Bucci, S. (2020). Confinement of air in the asian monsoon anticyclone and pathways of convective air to the stratosphere during the summer season. *Atmospheric Chemistry and Physics*, *20*(18), 11045–11064.

Munchak, L. A., & Pan, L. L. (2014). Separation of the lapse rate and the cold point tropopauses in the tropics and the resulting impact on cloud top-tropopause relationships. *Journal of Geophysical Research: Atmospheres*, *119*(13), 7963–7978.

Pan, L. L., Atlas, E. L., Salawitch, R., Honomichl, S., Bresch, J., Randel, W., ... others (2017). The convective transport of active species in the tropics (contrast) experiment. *Bulletin of the American Meteorological Society*, *98*(1), 106–128.

Pan, L. L., Bowman, K. P., Atlas, E. L., Wofsy, S. C., Zhang, F., Bresch, J. F., ... others (2010). The stratosphere–troposphere analyses of regional transport 2008 experiment. *Bulletin of the American Meteorological Society*, *91*(3), 327–342.

Pan, L. L., Honomichl, S. B., Kinnison, D. E., Abalos, M., Randel, W. J., Bergman, J. W., & Bian, J. (2016). Transport of chemical tracers from the bound-

ary layer to stratosphere associated with the dynamics of the asian summer monsoon. *Journal of Geophysical Research: Atmospheres*, *121*(23), 14–159.

Pan, L. L., Kinnison, D., Liang, Q., Chin, M., Santee, M. L., Flemming, J., ... others (2022). A multimodel investigation of asian summer monsoon utls transport over the western pacific. *Journal of Geophysical Research: Atmospheres*, *127*(24), e2022JD037511.

Park, M., Randel, W. J., Gettelman, A., Massie, S. T., & Jiang, J. H. (2007). Transport above the asian summer monsoon anticyclone inferred from aura microwave limb sounder tracers. *Journal of Geophysical Research: Atmospheres*, *112*(D16).

Park, M., Randel, W. J., Kinnison, D. E., Garcia, R. R., & Choi, W. (2004). Seasonal variation of methane, water vapor, and nitrogen oxides near the tropopause: Satellite observations and model simulations. *Journal of Geophysical Research: Atmospheres*, *109*(D3).

Ploeger, F., Konopka, P., Günther, G., Grooß, J.-U., & Müller, R. (2010). Impact of the vertical velocity scheme on modeling transport in the tropical tropopause layer. *Journal of Geophysical Research: Atmospheres*, *115*(D3).

Ploeger, F., Konopka, P., Walker, K., & Riese, M. (2017). Quantifying pollution transport from the asian monsoon anticyclone into the lower stratosphere. *Atmospheric Chemistry and Physics*, *17*(11), 7055–7066.

Plumb, R. A., & Ko, M. K. (1992). Interrelationships between mixing ratios of long-lived stratospheric constituents. *Journal of Geophysical Research: Atmospheres*, *97*(D9), 10145–10156.

Randel, W. J., Park, M., Emmons, L., Kinnison, D., Bernath, P., Walker, K. A., ... Pumphrey, H. (2010). Asian monsoon transport of pollution to the stratosphere. *Science*, *328*(5978), 611–613.

Schwantes, R. H., Lacey, F. G., Tilmes, S., Emmons, L. K., Lauritzen, P. H., Walters, S., ... others (2022). Evaluating the impact of chemical complexity and horizontal resolution on tropospheric ozone over the conterminous us with a global variable resolution chemistry model. *Journal of Advances in Modeling Earth Systems*, *14*(6), e2021MS002889.

Strahan, S., Duncan, B., & Hoor, P. (2007). Observationally derived transport diagnostics for the lowermost stratosphere and their application to the gmi chemistry and transport model. *Atmospheric Chemistry and Physics*, *7*(9), 2435–2445.

Tang, W., Emmons, L. K., Worden, H. M., Kumar, R., He, C., Gaubert, B., ... others (2023). Application of the multi-scale infrastructure for chemistry and aerosols version 0 (musicav0) for air quality in africa. *Geoscientific Model Development Discussions*, *2023*, 1–34.

Toon, O. B., Maring, H., Dibb, J., Ferrare, R., Jacob, D. J., Jensen, E. J., ... others (2016). Planning, implementation, and scientific goals of the studies of emissions and atmospheric composition, clouds and climate coupling by regional surveys (seac4rs) field mission. *Journal of Geophysical Research: Atmospheres*, *121*(9), 4967–5009.

Ulanovsky, A., Yushkov, V., Sitnikov, N., & Ravengnani, F. (2001). The fozan-ii fast-response chemiluminescent airborne ozone analyzer. *Instruments and Experimental Techniques*, *44*, 249–256.

Viciani, S., Montori, A., Chiarugi, A., & D'Amato, F. (2018). A portable quantum cascade laser spectrometer for atmospheric measurements of carbon monoxide. *Sensors*, *18*(7), 2380.

Villamayor, J., Iglesias-Suarez, F., Cuevas, C. A., Fernandez, R. P., Li, Q., Abalos, M., ... others (2023). Very short-lived halogens amplify ozone depletion trends in the tropical lower stratosphere. *Nature Climate Change*, 1–7.

Vogel, B., Günther, G., Müller, R., Grooß, J.-U., & Riese, M. (2015). Impact of different asian source regions on the composition of the asian monsoon anticy-

clone and of the extratropical lowermost stratosphere. *Atmospheric chemistry and physics*, *15*(23), 13699–13716.

Vogel, B., Müller, R., Günther, G., Spang, R., Hanumanthu, S., Li, D., ... Stiller, G. P. (2019). Lagrangian simulations of the transport of young air masses to the top of the asian monsoon anticyclone and into the tropical pipe. *Atmospheric Chemistry and Physics*, *19*(9), 6007–6034.

von Hobe, M., Ploeger, F., Konopka, P., Kloss, C., Ulanowski, A., Yushkov, V., ... others (2021). Upward transport into and within the asian monsoon anticyclone as inferred from stratoclim trace gas observations. *Atmospheric Chemistry and Physics*, *21*(2), 1267–1285.

Yan, X., Konopka, P., Ploeger, F., Podglajen, A., Wright, J. S., Müller, R., & Riese, M. (2019). The efficiency of transport into the stratosphere via the asian and north american summer monsoon circulations. *Atmospheric Chemistry and Physics*, *19*(24), 15629–15649.

Yin, M. T. (1949). Synoptic-aerologic study of the onset of the summer monsoon over india and burma. *Journal of Atmospheric Sciences*, *6*(6), 393–400.

Yushkov, V., Oulanovsky, A., Lechenuk, N., Roudakov, I., Arshinov, K., Tikhonov, F., ... Georgiadis, T. (1999). A chemiluminescent analyzer for stratospheric measurements of the ozone concentration (fozan). *Journal of Atmospheric and Oceanic Technology*, *16*(10), 1345–1350.

Zhang, G., & McFarlane, N. (1995). Sensitivity of climate simulations to the parameterization of cumulus convection in the canadian climate centre general circulation model. *Atmosphere Ocean*, *33*, 407–446.

Evaluating the Model Representation of Asian Summer Monsoon UTLS Transport and Composition using Airborne In Situ Observations

Warren P. Smith[1], Laura L. Pan[1], Douglas Kinnison[1], Elliot Atlas[2], Shawn Honomichl[1], Jun Zhang[1], Simone Tilmes[1], Rafael P. Fernandez[3], Alfonso Saiz-Lopez[4], Victoria Treadaway[5,6], Karina E. Adcock[7], Johannes C. Laube[8], Marc von Hobe[8], Corinna Kloss[8], Silvia Viciani[9], Francesco D'Amato[9], C. Michael Volk[10], Fabrizio Ravegnani[11]

[1]Atmospheric Chemistry Observations & Modeling Laboratory, National Center for Atmospheric Research, Boulder, Colorado, USA
[2]Department of Atmospheric Sciences, Rosenstiel School of Marine, Atmospheric, and Earth Science, University of Miami, Miami, Florida, USA
[3]Institute for Interdisciplinary Science (ICB), National Research Council (CONICET), FCEN-UNCuyo, Mendoza, Argentina
[4]Department of Atmospheric Chemistry and Climate, Institute of Physical Chemistry Blas Cabrera, CSIC, Madrid, Spain
[5]Cooperative Institute for Research in Environmental Sciences, University of Colorado Boulder, Boulder, Colorado, USA
[6]NOAA Chemical Sciences Laboratory, Boulder, Colorado USA
[7]Centre for Ocean and Atmospheric Sciences, School of Environmental Sciences, University of East Anglia, Norwich, UK
[8]Institute for Energy and Climate Research (IEK-7), Forschungszentrum Jülich GmbH, 52425 Jülich, Germany
[9]National Research Council - National Institute of Optics (CNR-INO), Sesto Fiorentino, Italy
[10]University of Wuppertal, Germany
[11]Institute of Atmospheric Sciences and Climate, Bologna, Italy

Key Points:

- We develop process-based diagnostics for model evaluation using airborne in situ observations
- We analyze the representation of the Asian summer monsoon for its role in impacting composition and climate
- The established diagnostics use dynamical and chemical coordinates to identify areas for model improvement

Corresponding author: Warren P. Smith, `wsmith@ucar.edu`

Abstract

Chemistry transport models (CTMs) are essential tools for characterizing and predicting the role of atmospheric composition and chemistry in Earth's climate system. This study demonstrates the use of airborne in situ observations to diagnose the representation of atmospheric composition by global CTMs. Process-based diagnostics are developed which minimize the spatial and temporal sampling differences between airborne in situ measurements and CTM grid points. The developed diagnostics make use of dynamical and chemical vertical coordinates as a means of highlighting areas where focused model improvement is needed. The chosen process is the chemical impact of the Asian summer monsoon (ASM), where deep convection serves a unique pathway for rapid transport of surface emissions and pollutants to the stratosphere. Two global CTM configurations are examined for their representation of the ASM upper troposphere and lower stratosphere (UTLS), using airborne observations collected over south Asia. Application of the developed diagnostics to the CTMs reveals the limitations of zonally-averaged surface boundary conditions for species with sufficiently short tropospheric lifetimes, and that species whose stratospheric loss rates are dominated by photolysis have excellent agreement compared to that observed. Overall, the diagnostics demonstrate the strength of airborne observations toward improving model predictions, and highlight the utility of high-resolution climate modeling to improve the understanding of reactive transport of anthropogenic pollutants to the stratosphere.

Plain Language Summary

The chemical composition of Earth's atmosphere has important implications for the health of all its ecosystems. This study establishes an approach for evaluating the representation of chemical composition in global climate models, and demonstrates the capabilities of the approach using a set of observations collected by research aircraft. We specifically focus the evaluation on the Asian summer monsoon, a region with a known pathway for transport of chemical species from near the surface into the upper atmosphere. In doing so, we identify specific areas where focused model improvement is needed.

1 Introduction

The chemical composition of Earth's atmosphere has implications for its climate and the health of all its ecosystems. Changes in atmospheric composition, induced by changes in both natural processes and anthropogenic activities, may have impacts on surface air quality, the atmosphere's energy budget, the delay of stratospheric ozone recovery as set in motion by the Montreal Protocol, among others. As such, ensuring the accurate characterization and prediction of past, present and future atmospheric composition remains a compelling research avenue.

Chemistry-climate models (CCMs) are commonly used tools to characterize and predict atmospheric composition. This type of model often sacrifices horizontal grid spacing (typically tens to hundreds of kilometers) in favor of simulating extended time periods (years to decades) with global coverage (e.g., Danabasoglu et al., 2020). Trust in any model to accurately predict the future fundamentally hinges upon its adequate representation of the past and present. Often CCMs are evaluated with satellite products and monitoring station observations using time- (e.g., monthly) or spatially- (e.g., zonal average or prescribed regions) averaged comparisons (e.g., Gettelman et al., 2019; Bossolasco et al., 2021; Strahan et al., 2007; Froidevaux et al., 2019). Despite the known impact of regional-scale processes on atmospheric composition and climate, these processes must typically be parameterized in CCMs because their spatial (on the order of kilometers) and temporal (on the order of hours) scales are not compatible with a typical CCM's grid configuration. To evaluate and improve the representation of regional-scale processes

in CCMs, it is necessary to evaluate them for shorter time periods or for specific regions. In this configuration, a CCM is integrated as a chemistry transport model (CTM).

Airborne field campaigns for targeted regions and/or specific phenomena can provide observations to elucidate regional-scale processes affecting atmospheric composition (e.g., Pan et al., 2010, 2017; Toon et al., 2016). Airborne instruments have the capability to sample a portion of the atmosphere in unparalleled detail given their high sampling frequency. However, the high spatial and temporal resolution over a confined area fall into sharp contrast with the grid structures of CTMs, which can make their application for model evaluation difficult to reconcile. Global CTMs typically use horizontal grid spacing of tens or hundreds of kilometers, making them much coarser than airborne in situ observations which are often spaced at hundreds or thousands of meters. As such, specific diagnostic tools are needed to minimize the fundamental differences in air mass sizes represented by in situ observations and CTMs. A straightforward technique is to interpolate a flight track onto a CTM's grid and compare this with observations taken along the same flight track, but given the aforementioned disparities in air mass sizes this approach may underutilize the full capabilities of both the observations and model.

The goal of this study is to demonstrate the use of airborne in situ observations to diagnose CTM representation of deep convective transport to the UTLS and subsequent stratospheric loss processes. Specifically, we present newly-developed process-based diagnostics which use both dynamical and chemical coordinates to minimize the fundamental differences in air mass sizes represented by airborne in situ observations and CTMs. Surface boundary conditions (i.e., surface mixing ratios), dynamics, and chemistry are all considered in the diagnostic development. In doing so, we demonstrate the wealth of information contained within airborne in situ observations, and show that this approach of connecting observations and models enhances the value of each.

The specific process of the present evaluation is the Asian summer monsoon (ASM), a dominant weather system during boreal summer which has long been known for its generation of seasonal rainfall over portions of Asia (e.g., Yin, 1949). The line of research we focus on in this work concerns the air mass that is transported from the Asian boundary layer (BL) through ASM deep convection and its subsequent transport. Specifically, water vapor and tropospheric pollutants can be transported vertically through convection to reach the upper troposphere and lower stratosphere (UTLS), where they have the potential to impact global atmospheric composition and climate (e.g., Dethof et al., 1999; Fu et al., 2006; Chen et al., 2012; Fan et al., 2017). The application of chemical and transport modeling techniques to predict ASM impacts on global atmospheric composition remains an active research area (e.g., Ploeger et al., 2017; Vogel et al., 2019; Yan et al., 2019; Pan et al., 2016, 2022; Clemens et al., 2023).

The dynamical response to ASM deep convection, an anticyclone which forms in the UTLS during boreal summer (Krishnamurti & Bhalme, 1976), has been observed by satellite to show confinement of anomalous pollutant concentrations of anthropogenic signature (e.g., Park et al., 2004, 2007; Randel et al., 2010). Tropopause altitudes over the ASM are typically higher than the surrounding regions, so ASM pollutants detrained from deep convection may be subsequently transported to the stratosphere through quasi-isentropic mixing as they spiral upward anticyclonically (e.g., Pan et al., 2016; Vogel et al., 2019; Legras & Bucci, 2020). Short-lived halogenated species transported to the UTLS in this way may delay the recovery of stratospheric ozone (e.g., Bednarz et al., 2022), where the modeled impact depends on the complexity of the chemical mechanism or treatment considered (Fernandez et al., 2021). The potential for the ASM to impact atmospheric composition and climate makes it an ideal setting for the development of CTM evaluation diagnostics.

Table 1. A collection of StratoClim data used for the development of model diagnostics in this study, including the sensors or instruments that obtained them.

Instrument	Species Used	PI	Reference
AMICA	Carbon Monoxide (CO)	M. von Hobe	Kloss et al. (2021)
COLD2	Carbon Monoxide (CO)	S. Viciani	Viciani et al. (2018)
FOZAN-II	Ozone (O_3)	F. Ravegnani	Ulanovsky et al. (2001)
HAGAR	Nitrous Oxide (N_2O)	C. M. Volk	Homan et al. (2010)
WAS	Halogenated Species	J. Laube	Adcock et al. (2021)

The model evaluation and diagnostic development is broken down into three specific processes which loosely encompass the pathway for anthropogenic pollution emitted over Asia to impact UTLS composition, and thus global climate. Each analyzed process results in the development of a diagnostic, and is presented in its own subsection within Section 3. First, we use an adjusted-tropopause relative altitude coordinate to diagnose transport of polluted air masses from the Asian BL to the ASM UTLS anticyclone via deep convection (Section 3.1). Next, we diagnose the modeled mixing ratios of halogenated species as they cross the ASM tropopause and enter the stratosphere (Section 3.2). Finally, we diagnose model chemical loss rates in the stratosphere by using the mixing ratio of long-lived tracers as a vertical coordinate (Section 3.3). To demonstrate the value of the diagnostic development, we evaluate two CTMs with different grid configurations (Section 2.2) by using a set of airborne in situ observations taken over south Asia during the ASM's active period (Section 2.1).

2 Tools for Diagnostic Development

2.1 Airborne in situ observations from StratoClim 2017

Motivated by the pronounced impacts of the ASM on UTLS composition, the StratoClim airborne field campaign (http://www.stratoclim.org/; von Hobe et al., 2021; Bucci et al., 2020) was conducted during boreal summers 2016 and 2017 with bases in Kalamata, Greece and Kathmandu, Nepal, respectively. As the 2017 deployment took place over southern Asia, the region identified as the predominant source of convective uplift for the ASM UTLS anticyclone (e.g., Bergman et al., 2013; Vogel et al., 2015; Pan et al., 2016), we use only the 2017 observations throughout this paper, and henceforth refer to this deployment as "the StratoClim campaign" for simplicity. The StratoClim campaign conducted eight research flights onboard the M55 Geophysica between July 27 and August 10, 2017. The location of the experiment is shown in Figure 1 with dynamical context. The research flights primarily sampled the interior of the ASM UTLS anticyclone (e.g., Figure 1 of von Hobe et al., 2021). Here we also show the flight tracks relative to the seasonal location of the anticyclone from a geopotential height perspective (panel a) as well as in pressure (panel b) and potential temperature (panel c) space.

We use chemical observations obtained by several airborne instruments onboard the M55 Geophysica for the diagnostic development herein. The measurements are summarized in Table 1, and we direct the reader to the listed references for specifics about the instruments. In the interest of being thorough, we include a few pertinent details below.

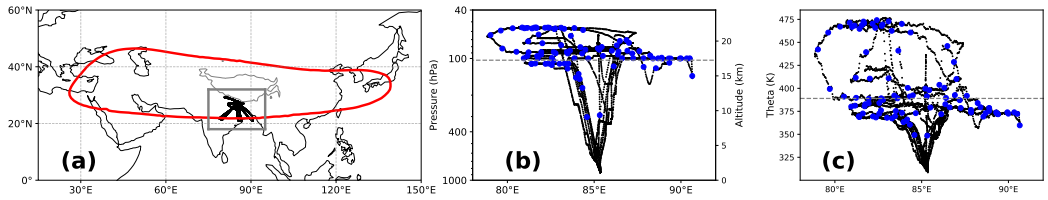

Figure 1. Setting of the StratoClim 2017 experiment with flight tracks shown in black. In panel a, the red contour shows the geopotential height contour of 16.77 km at 100 hPa (threshold taken from Bian et al., 2012) from Global Forecasting System (GFS) analysis averaged over the StratoClim measurement period, and the gray box shows the domain which the models are subset to throughout Section 3. Panels b and c show the flight tracks in vertical perspective using pressure, altitude and potential temperature vertical coordinates. Whole Air Sampler (WAS) observation points marked in blue, and dashed gray lines denote the mean tropopause during the StratoClim sampling period.

2.1.1 AMICA Carbon Monoxide

Observations of the tropospheric-sourced trace gas carbon monoxide (CO) are used to diagnose properties of convective transport. We use CO observations from the Airborne Mid-Infrared Cavity enhanced Absorption spectrometer (AMICA, Kloss et al., 2021), which was deployed for the first time during the StratoClim campaign. These data are available on 10 second intervals, are estimated to have an overall accuracy of better than 5% and a 1σ precision of $\sim$20 ppb. These data have been previously analyzed toward understanding the dynamical and transport properties of the ASM by von Hobe et al. (2021).

2.1.2 COLD2 Carbon Monoxide

We also include CO observations from the Carbon Oxide Laser Detector 2 (COLD2, Viciani et al., 2018) instrument. COLD2 observations have a higher sampling frequency, with data available on a 1 second interval. The CO mixing ratio accuracy is estimated to be 3%. The COLD2 instrument has now been deployed for two ASM-centric campaigns: both StratoClim and the Asian summer monsoon Chemical and Climate Impact Project (ACCLIP 2022, Pan et al., 2022).

2.1.3 FOZAN-II Ozone

Ozone (O_3) is commonly used as a stratospheric tracer, making it an important component of the diagnostic development herein. We use observations of ozone taken from the Fast OZone ANalyzer (FOZAN-II, Yushkov et al., 1999; Ulanovsky et al., 2001) during six of the eight StratoClim flights in 2017. FOZAN-II sampling time is 1 second, the sensitivity is about 1 ppbv, and the average accuracy is 7%.

2.1.4 HAGAR Nitrous Oxide

We use observations of nitrous oxide (N_2O) due to its long tropospheric lifetime (15,600 years, SPARC Report No. 6), making it ideal to use as a chemical vertical coordinate in the stratosphere. This was measured during StratoClim by the High Altitude Gas AnalyzeR (HAGAR, Homan et al., 2010). The measurements have a 90 second sampling interval, an average precision of $\sim$0.5% and an average accuracy of $\sim$0.6%.

2.1.5 WAS Halogenated Species

To assess the modeled chemical mechanisms, we make use of air samples collected by a Whole Air Sampler (WAS) during StratoClim, which were subsequently analyzed for a wide range of halogenated species (Adcock et al., 2021). Selected species for this study include methyl halides, (hydro)chlorofluorocarbons ((H)CFCs), with a focus on species emphasized in Adcock et al. (2021) due to their ready availability. These species are produced by both natural and anthropogenic activities, and if lofted to the stratosphere can lead to the catalytic destruction of ozone. Each StratoClim flight included a maximum of 20 WAS samples, each with sampling duration of a few minutes. The sampling was performed on a non-uniform time grid, as depicted in Figure 1 (blue dots in panels b and c). Uncertainty information from each sample is provided via Adcock et al. (2021). "Merged" datasets onto the WAS measurement time interval are used in Section 3 to account for the irregular sampling intervals for this instrument. This is done by averaging all observations that fall between a given WAS canister's open and close times.

2.2 Chemistry Transport Model Configurations

Use of the diagnostics developed herein is demonstrated using two atmosphere model components within the NCAR Community Earth System Model version 2 (CESM2, Danabasoglu et al., 2020). The first model is the Whole Atmosphere Community Climate Model version 6 (WACCM6, Gettelman et al., 2019) which uses a 0.95° latitude x 1.25° longitude grid with 110 vertical levels spanning from the surface to ∼140km (Garcia and Richter, 2019). This vertical level configuration gives WACCM a vertical grid spacing of ∼500 m in the UTLS. The second model is the recently-developed MUlti-Scale Infrastructure for Chemistry and Aerosols version 0 (MUSICAv0, Schwantes et al., 2022), which has the capability for user-customized horizontal grid refinement to improve sampling over a region of interest. For the current work, a custom MUSICA grid is developed with refinement to ∼30 km horizontal spacing over southeastern Asia and the western north Pacific (Figure S1a), while the remainder of the globe is covered by ∼1° spacing (similar to WACCM). The MUSICA grid uses 32 vertical levels spanning from the surface to ∼80km (∼3 hPa), resulting in a ∼1km vertical grid spacing in the UTLS. The vertical grid increments in WACCM and MUSICA are shown in Figure S1b. Output from the WACCM (MUSICA) simulation is available on 3- (6-) hour intervals.

Both WACCM and MUSICA utilize a specified dynamics option which nudges the temperature and zonal and meridional wind components to a chosen meteorological analysis. For this we use the Modern-Era Retrospective analysis for Research and Applications version 2 (MERRA-2, Gelaro et al., 2017). Global surface emissions are provided by the Copernicus Atmosphere Modeling System (CAMS, Granier et al., 2019). The chemistry mechanism in CESM2 includes a total of 231 species and 538 chemical reactions and is described by Emmons et al. (2020). The simulations parameterize deep convection using the Zhang-McFarlane scheme (Zhang & McFarlane, 1995). Other parameterizations are given by Gettelman et al. (2019) and are omitted here for brevity.

Advancements in computational processing and storage capabilities in recent years have enabled developments in finer grid spacing (i.e., higher resolution) and multi-scale grid capabilities in CTMs, such as MUSICA. In the present study, the MUSICA grid refinement is chosen to encompass the southern flank of the Tibetan Plateau (see Figure S1a), the primary "conduit" for ASM deep convective transport into the UTLS (e.g., Bergman et al., 2013; Honomichl & Pan, 2020; Clemens et al., 2023), with the intent to improve the representation of convective-scale processes responsible for lofting BL pollutants into the ASM UTLS. It remains unclear, however, whether improved grid point sampling necessarily improves a model's performance compared to a coarser-grid counterpart. This supports the establishment of process-based model evaluation diagnostics as a timely research area.

To illustrate the important role of the ASM in modifying UTLS composition, Figure 2 shows global map sections of selected chemical species from WACCM valid 500 m above the local model tropopause. A pronounced chemical signature of trace gases associated with the ASM UTLS anticyclone can be seen, similar to that of past observational and modeling studies (e.g., Park et al., 2007; Randel et al., 2010; Munchak & Pan, 2014; Pan et al., 2022), but now with consideration for filtering for a "bulging" tropopause structure over the ASM (Pan et al., 2016). The result indicates that species with tropospheric lifetimes in months (top row) have mixing ratios in the lowermost stratosphere that are larger over the ASM than anywhere else on Earth, underscoring the potential for short-lived halogenated species emitted over Asia to impact the composition of the stratosphere via the ASM transport mechanism discussed in Section 1. In contrast, species with much longer tropospheric lifetimes (bottom row) show similar mixing ratio enhancements over south Asia as in the tropical tropopause layer (TTL, Fueglistaler et al., 2009). These species are well-mixed throughout the troposphere, but begin to decay in the lower stratosphere as transport times grow longer and their chemical sinks grow stronger. Their

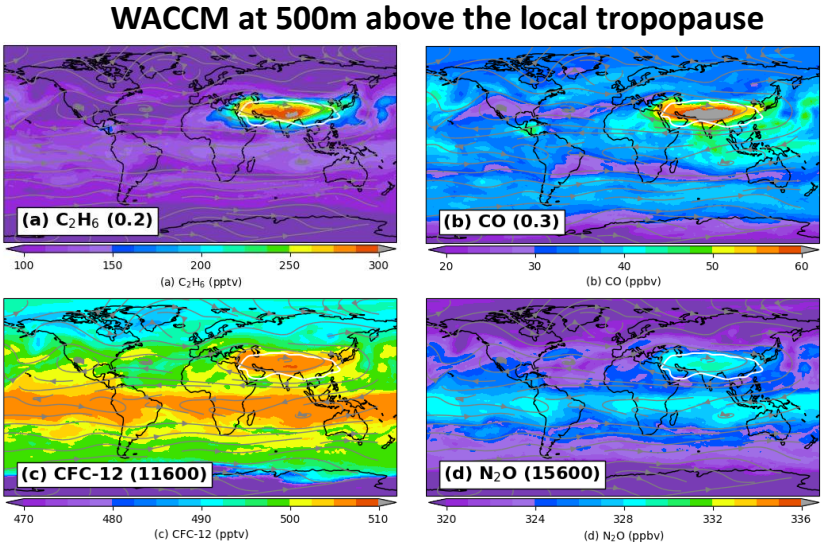

Figure 2. Plan views of WACCM model chemical species and dynamical variables in the lowermost stratosphere during the StratoClim observation period. Ethane (C_2H_6), carbon monoxide (CO), CFC-12 (CCl_2F_2) and nitrous oxide (N_2O) averaged from July 27 – August 10, 2017 and 500 m above the local WACCM tropopause are shown. White contours show WACCM tropopause altitudes greater than 16.77 km and gray lines show wind streamlines. Respective tropospheric lifetimes from SPARC Report No. 6 are given in parentheses.

highest mixing ratios in Figure 2 are simply regions where there is net upward transport across the tropopause: the TTL and the ASM.

3 Process-based Diagnostic Development and Evaluation Demonstration

3.1 Transport by Monsoon Deep Convection

Deep convection associated with the ASM is responsible for redistributing natural and anthropogenic pollutants from the BL into the UTLS (e.g., Fu et al., 2006). In this section we use high-resolution airborne data to diagnose the convective parameterization in WACCM and MUSICA (Zhang and McFarlane, 1995) by evaluating how well a tropospheric and stratospheric tracer (CO and ozone, respectively) are distributed throughout the free troposphere and UTLS compared to observations.

To examine vertical transport of CO and ozone, vertical distributions of the StratoClim observations and model results for South Asia are shown in Figure 3. Tracer mixing ratios are compared using two different vertical coordinates: adjusted tropopause-relative altitude, which expands the tropospheric layer and highlights the air mass transition across the tropopause, and potential temperature, which collapses the tropospheric layer to highlight the transition between convective-dominated and radiative-dominated ascent processes. The lapse rate tropopause (LRT) altitude from ERA5 reanalysis (Hersbach et al., 2020; Hoffmann & Spang, 2022) is interpolated to the flight tracks for observations, while the model-derived LRT is used for WACCM and MUSICA. The tropopause-relative altitude coordinate has utility for understanding the behavior of ASM convective transport relative to the tropopause, and enables adjustment for subtle differences

between model dynamics and those in the real atmosphere. This analysis is complementary to and extends that of von Hobe et al. (2021), by analyzing how models represent tracer behavior in the ASM region.

The result shows that MUSICA and WACCM have a generally good agreement with CO observations from AMICA and COLD2, mixing ratios ranging from ∼70-140 ppbv throughout the troposphere and gradually decreasing to ∼15-30 ppbv in the lower stratosphere in both observations and models (Figure 3, left panels). CO observations have a similar distribution of CO throughout the majority of free tropospheric altitudes, suggesting that convection is the dominant transport process up to ∼1-2 km below the local tropopause (∼15km altitude on average). Separate maxima in modeled CO in the lower and upper troposphere show the influence of shallow and deep convective modes of transport, respectively. In potential temperature space, the noticeable discontinuity at ∼360K clearly reveals the transition from convective-dominated to radiative-dominated ascent.

On the other hand, MUSICA and WACCM struggle to represent the observed distribution of ozone, with a high bias spanning between the free troposphere and lower stratosphere (Figure 3, right panels). This is not particularly surprising, as WACCM and MUSICA ozone has been noted to have a high bias in previous work when compared to observations (Froidevaux et al., 2019; Dubé et al., 2022; Tang et al., 2023). Ozone mixing ratios observed by FOZAN-II are further supported by ozonesonde observations over Nepal during StratoClim, which show ∼30-50 ppbv ozone throughout the free troposphere (Brunamonti et al., 2018). We have performed several sensitivity experiments to elucidate the cause of the model high bias, including testing for sensitivity to chemistry of very short lived (VSL) species using the model configuration of Villamayor et al. (2023), and to adjusting the model's lightning parameterization to generate less NOx (an ozone precursor). The results of these sensitivity runs on model ozone mixing ratios shown in Figure S3. Although these experiments reduce the model's ozone, they do not explain a sufficiently large bias to close the gap with the observations. More generally, these sensitivity experiments demonstrate another application of the dynamical coordinate diagnostic, highlighting its utility in interrogating modeled representations of tracer mixing ratios.

A critical component to the analysis presented in Figure 3 is that model distributions are computed from broader spatial and temporal boundaries compared to the StratoClim flight tracks. Specifically, the model distributions are an average of all grid points between 75-95°E longitude, 18-32°N latitude (the gray box printed on Figure 1a), and at every 3- or 6-hour interval between July 27 – August 10, 2017. Instead of comparing each observation to a much larger model grid cell through interpolation (we demonstrate this common technique in Figure S2 for context), our technique allows a comparison of the general behavior of ASM transport throughout the monsoon's active phase. We acknowledge that flight campaigns often bias their sampling to specific phenomenon (e.g., convective complexes, wildfire plumes, etc.) which could complicate the interpretation of this evaluation, however most StratoClim flights were designed to survey the large-scale characteristics of the ASM UTLS, which supports the compatibility of this evaluation technique (Bucci et al., 2020).

To demonstrate an additional use of the dynamical vertical coordinates used in this analysis, we compare distributions of the tropospheric tracer CO in Figure 4 at key vertical layers identified from analyzing Figure 3. This allows for a more quantitative evaluation of the models against the observations, as well as a quantitative comparison of the WACCM and MUSICA grid configurations following the discussion in Section 2.2. The general similarity between observations and models at each of the selected layers corroborates with the qualitative agreement noted in Figure 3. Mean values from the distributions are collected in Table 2.

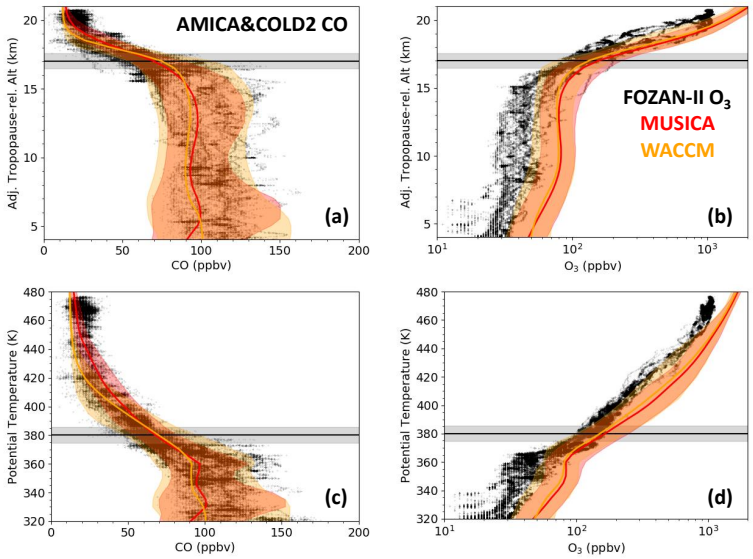

Figure 3. Vertical profile distributions of modeled and observed (left) CO and (right) ozone mixing ratio vertical profiles from models and StratoClim observations. The top panels are plotted in tropopause-relative altitude space while the bottom panels are plotted in potential temperature space. Black dots show StratoClim observations, and MUSICA (WACCM) results are plotted in red (orange), where solid lines show the mean and shaded regions show the 5th to 95th percentile range. The tropopause is denoted by the solid black line with its standard deviation marked by gray shading. Y-axes in the top panels are "adjusted" by the mean tropopause value for ease of comprehension. Model output is restricted to 75-95 E, 18-32 N (gray box in Figure 1a) from July 27 - August 10, 2017.

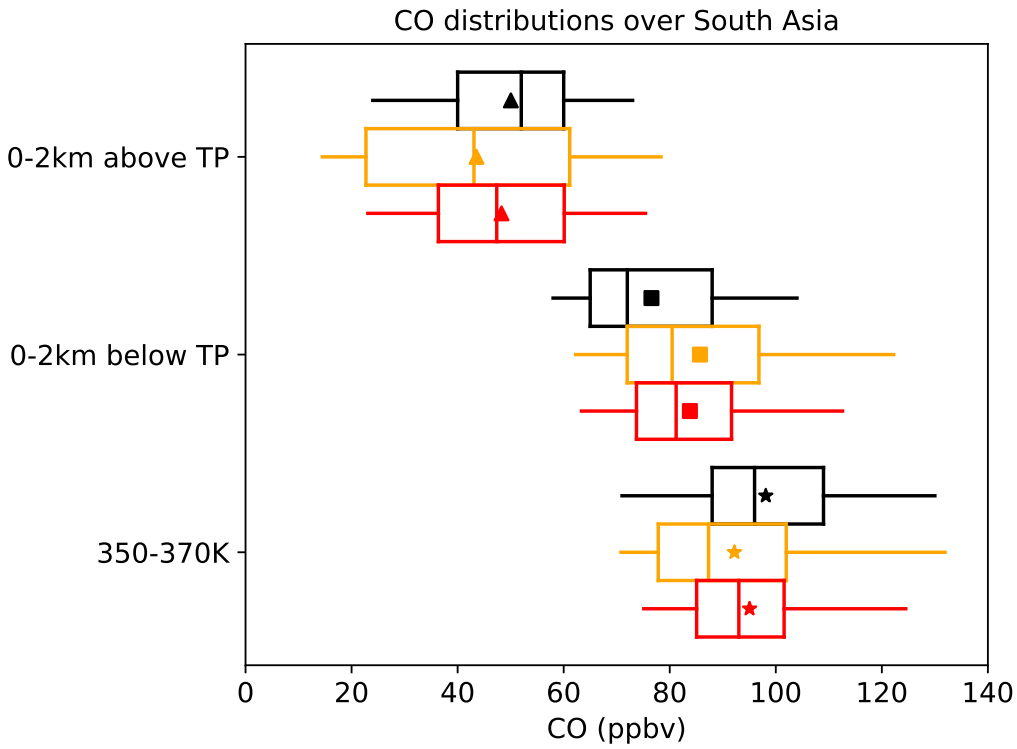

Figure 4. Box and whisker plots for CO mixing ratios within selected vertical ranges, with observations from AMICA and COLD2 in black, WACCM in orange, and MUSICA in red. "Boxes" span from the 25th to 75th percentiles, "whiskers" span from the 5th to 95th percentiles, and the vertical lines in the "boxes" represent the median. Mean mixing ratios are plotted as triangles (squares) for 0 to 2km above (below) the local tropopause (abbreviated as "TP" on the y axis), and as stars for 350 K to 370 K potential temperature.

There is no obvious advantage demonstrated by the MUSICA simulation with refined horizontal grid spacing at the level of primary convective outflow (stars in Figure 4 and Table 2). This may be because convection must still be parameterized with the MUSICA grid configuration. Interestingly however, CO mixing ratios distributions in the lowermost stratosphere (triangles in Figure 4 and Table 2) suggest a low bias compared to observations. Although the present work does not pursue model improvements to address these discrepancies, the examples provided here are evidence for how the diagnostics using these dynamical coordinates may identify specific areas for targeted model interrogation and development.

3.2 Transport Across the ASM Tropopause

Polluted air masses lofted by deep convection may be deposited higher than the level of zero radiative heating (LZRH, ∼360K in the tropics, Ploeger et al., 2010), above which air masses preferentially undergo comparatively slow ascent. Polluted air masses which cross the ASM tropopause, either vertically or through quasi-isentropic transport to the surrounding lower-tropopause regions (e.g., Pan et al., 2016; Vogel et al., 2019), may thus have the potential to impact global composition and climate. Modeling the appropriate mixing ratios of pollutants at the ASM tropopause is thus an important com-

Table 2. Mean CO mixing ratios (ppbv) in each selected vertical range shown in Figure 4.

Layer Symbol	0-2 km above LRT Triangle	0-2 km above LRT Square	350-370 K θ Star
AMICA/COLD2	43.2	69.4	98.1
WACCM	43.6	85.7	92.2
MUSICA	48.3	83.8	95.1

ponent of representing the ASM's impacts. This section diagnoses the model representation of halogenated species and N_2O mixing ratios in the ASM tropopause layer.

Selected halogenated species and N_2O from WACCM, MUSICA, and StratoClim airborne observations from the WAS and HAGAR instruments (respectively) are shown in Figure 5. As in Section 3.1, we use an adjusted tropopause-relative coordinate to adjust for dynamical differences in models compared to that in the real atmosphere. The result shows that the models have qualitatively good representation of the four selected species at the ASM tropopause. For species with tropospheric lifetimes longer than one year, tropospheric mixing ratios are nearly constant with altitude given this is long compared to typical overturning of the troposphere (typically 2-3 weeks). Thus, their mixing ratio accuracy at the tropopause is mainly controlled by the model's lower boundary condition used to prescribe surface mixing ratios. We note there is a slight high bias in modeled mixing ratios found ∼2-3 km above the local tropopause in all panels of Figure 5. This suggests an error in the behavior of model dynamics in the lower stratosphere, either through vertical motion or mixing from the surrounding regions. The model representation of the lower stratosphere will be addressed in more detail in Section 3.3.

Although the modeled species tropopause mixing ratios depicted in Figure 5 are qualitatively encouraging, we wish to establish a quantitative diagnostic to characterize the error in modeled stratospheric entry mixing ratios, to easily identify species which are simulated (in)adequately. For this, we calculate the mean observed and modeled mixing ratios near the local tropopause (we choose within 1 km above and below; see the gray regions in Figure 5) and compare their difference against the "observational range of variability", to characterize biases which are large compared to the mixing ratio range throughout the ASM UTLS. Put mathematically:

$$Stratosphere\ Entry\ Error = \frac{q_{t,m} - q_{t,o}}{\Delta q_o} * 100\% \quad (1)$$

where q is the mixing of a given specie, the subscript t indicates the mean mixing ratio within 1 km of the local tropopause (as shown in Figure 5) during the StratoClim period, and the subscript m (o) indicates modeled (observed). Δq_0 is the difference between the maximum and minimum observed mixing ratio in the entire StratoClim dataset (i.e., the "observational range of variability"). The results are shown in Figure 6.

The calculation of error statistics, as done in Figure 6, provides a conceptual framework for identifying model skill in species representation, concisely highlighting areas where focused model development is needed. It also allows for different model configurations to be compared relative to one another. In the current approach, we see mostly superficial differences between WACCM and MUSICA in their stratospheric entry mixing ratio performance, likely a consequence of the same emissions database used in the simulations. Most species have stratospheric entry mixing ratio errors which are less than 10%, which we consider to be small given they could be easily explained by a combination of measurement and model uncertainties as well as the intentional sampling differ-

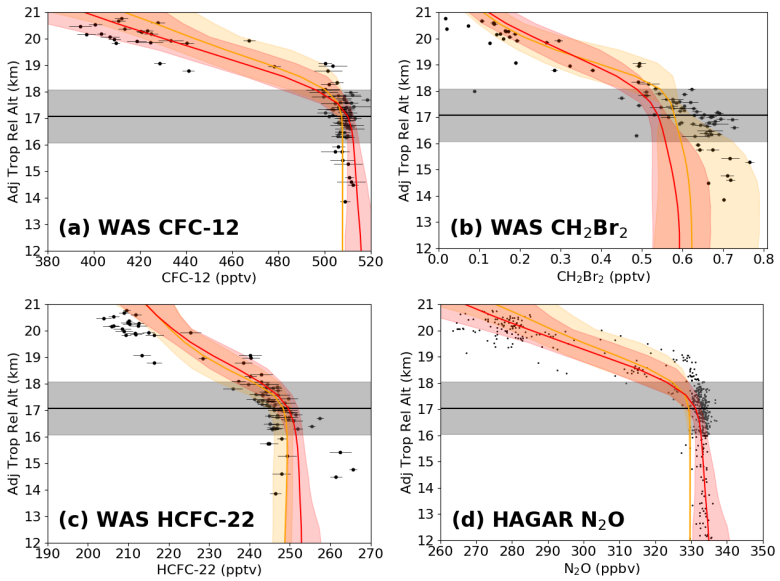

Figure 5. Modeled and observed vertical profiles of selected chemical species plotted in adjusted tropopause-relative altitude space. Black dots show observations with uncertainty plotted in thin horizontal lines. The red (orange) line shows the mean profile from the MUSICA (WACCM) simulation between 75-95E and 18-32N (the small gray box in Figure 1) from July 27 - August 10, 2017, with the corresponding shading spanning the 5th to 95th percentiles. The mean tropopause is shown as a black line, with the range of 1 km below and above it (used for calculation of the "stratospheric entry value") shaded in gray. As in Figure 3, y-axes are "adjusted" to the mean tropopause altitude for ease of comprehension.

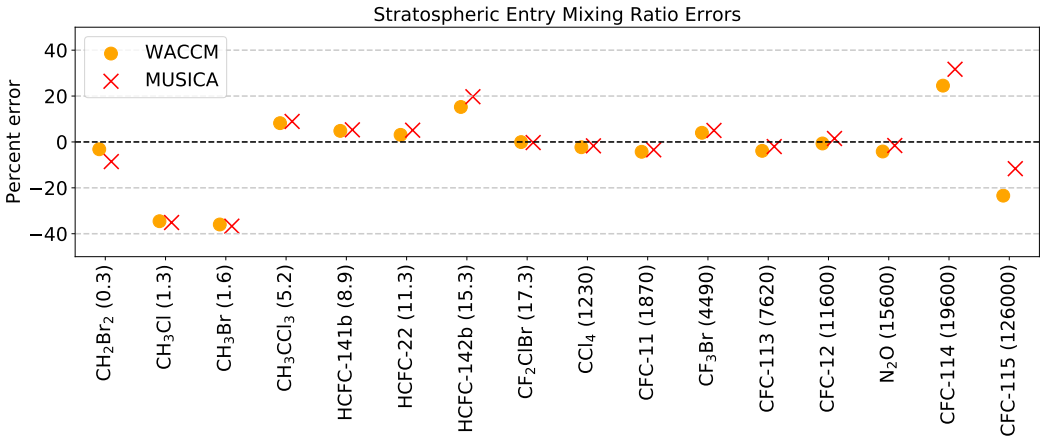

Figure 6. A scatterplot of model stratospheric entry errors for selected species. Species are sorted by their tropospheric lifetimes (SPARC Report No. 6) which are printed in parentheses in units of years.

ences we use to avoid space-time interpolation. However, this diagnostic identifies methyl chloride (CH_3Cl), methyl bromide (CH_3Br), CFC-114, and CFC-115 as species with larger errors which may have other contributing factors. Methyl chloride and bromide are of particular interest because although their tropospheric lifetimes are on the order of one year, their stratospheric lifetimes are on the order of decades (SPARC Report No. 6, Ko et al., 2013). Since these species will persist in the stratosphere for decades if they can penetrate the tropopause, and because of their impacts on stratospheric ozone chemistry (e.g., Bednarz et al., 2022), their mixing ratios in the ASM UTLS are especially important to properly represent.

To demonstrate the use of the stratospheric entry mixing ratio error calculation (Equation 1; Figure 6) in diagnosing model shortcomings, Figure 7 shows the methyl halides plotted in chemical vertical coordinate space. Both CO and CFC-12 are used as chemical coordinates to expand the tropospheric and stratospheric layers, respectively. The noticeable offsets between observed mixing ratios (black) and those from the models (red and orange) corroborate with their large errors (Figure 6). With the exception of dibromomethane (CH_2Br_2) which has the shortest tropospheric lifetime in this study, all the species analyzed in Figure 6 have mixing ratios prescribed at the model surface by using zonally-averaged mole fraction boundary conditions. Species with sufficiently long lifetimes relative to tropospheric overturning are expected to have nearly-uniform mixing ratios throughout the troposphere, as demonstrated by WACCM in Figure 2. However, for species with shorter tropospheric lifetimes such as methyl chloride and methyl bromide, this lower boundary condition may obscure important regional emissions sources, such as those from Asia, and lead to an underestimation of their composition and climate impact potentials.

The hypothesis that zonally-averaged mole fraction surface boundary conditions causes errors for methyl chloride and bromide at the stratospheric entry point can be further investigated by comparing WACCM and MUSICA results with observations outside the ASM region. For this we include in Figure 7 observations from the Studies of Emissions and Atmospheric Composition, Clouds and Climate Coupling by Regional Surveys (SEAC^{4}RS) campaign, which took place over North America during boreal summer 2013 (Toon et al., 2016), as gray dots. SEAC^{4}RS observations align nicely with the 2017 WACCM and MUSICA simulations subset to the ASM region (gray box in Figure

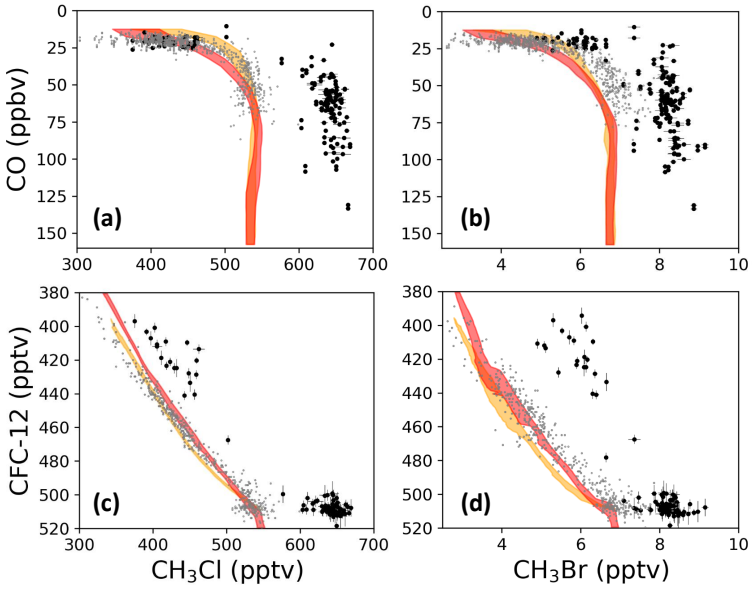

Figure 7. Vertical profiles of (left) methyl chloride and (right) methyl bromide in chemical coordinate space using (top) CO and (bottom) CFC-12 as the vertical coordinates. WACCM (MUSICA) mixing ratios from the 5th to 95th percentiles are shown in orange (red). Black dots show airborne observations from StratoClim (2017) with uncertainty bars, and gray dots show airborne observations from SEAC^{4}RS 2013 (Toon et al., 2016) taken over North America. To ensure compatibility between the campaigns, we adjust the CFC-12 mixing ratios from SEAC^{4}RS according to the long-term trend between 2013 and 2017, using observations from the NOAA/GML halocarbons program (Dutton et al., 2023).

1), indicating that model mixing ratios reflect the ASM's surroundings rather than the ASM environment itself. This supports our assertion that the prescribed zonally-averaged boundary condition assumption breaks down for species with tropospheric lifetimes less than a few years. More broadly, this analysis highlights the value of the stratospheric entry diagnostic at identifying model shortcomings and providing a pathway for focused improvements.

3.3 Chemical Loss in the Lower Stratosphere

The two previous sub-sections focus on transport of Asian pollution into the UT via convective transport (Section 3.1), and subsequent entry to the stratosphere (Section 3.2). In this sub-section we diagnose the model representation of chemical loss processes in the lower stratosphere, using a "chemical vertical coordinate." The relatively coarse vertical grid spacing in MUSICA which degrades further in the lower stratosphere (Figure S1b) leads us to focus this evaluation on the WACCM simulation only. Furthermore, due to the aforementioned issues with methyl halide species (Figures 6 and 7) and the inappropriateness of a linear fit for dibromomethane (CH_2Br_2; not shown), these species are excluded from this chemical loss analysis.

Following the approach of Avallone and Prather (1997), a collection of tracer relationships for halogenated species and N_2O are plotted in Figure 8 with CFC-12 mixing ratio used as the vertical coordinate for both WACCM and StratoClim observations. Although the full range of variability is plotted, we focus on the cluster of stratospheric observations between 394-442 pptv of CFC-12, to ensure the tracer relationships are con-

sistent with the observations. For this range of mixing ratios, linear "best fit" lines are calculated for both observations (black lines) and WACCM (brown lines). Measurement uncertainty (from Adcock et al., 2021) is accounted for by assigning weights to each point for the linear fitting, equal to the inverse of the sum of both the squared mixing ratio uncertainties. Furthermore, we discard two WAS data points (one for CCl_4 and another for CFC-114) which are clear outliers, and by inspection disrupt the appropriateness of the linear fit (not shown).

From the foundational arguments of Plumb and Ko (1992) on tracer relationships: "the curve becomes linear in any region if the net upward fluxes of two species through the rapid exchange surfaces in that region are in constant ratio." Indeed, the modeled and observed relationships exhibit linear behavior in the lower stratosphere (Figure 8), suggesting the species lifetimes are long in this layer compared to the timescales of net upward flux. From a conceptual standpoint, the chemical mechanism in WACCM has excellent representation of this behavior. In contrast, many relationships in Figure 8 exhibit non-linear behavior closer to the tropopause (∼500 pptv of CFC-12; see Figure 5), a consequence of the large lifetime disparity between the species on each axis. Often in these cases, the observations (gray dots) are considerably less compact than both WACCM (light orange dots) and their deeper stratospheric counterparts (black dots).

To quantify the ability of WACCM to represent the observed tracer relationships, a diagnostic is developed that is based on the modeled and observed chemical loss rate (i.e. slopes of the linear fitting). Often the WACCM loss rates are similar to those observed, but are "offset" in absolute mixing ratio (Figure 8). To calculate the loss rate and mixing ratio offset errors, we employ similar formulas as Equation 1 for the stratospheric entry mixing ratio errors:

$$Loss\ Rate\ Error = \frac{m_{ls,W} - q_{ls,o}}{\Delta m_{ls,0}} * 100\% \tag{2}$$

$$Mixing\ Ratio\ Offset\ Error = \frac{q_{ls,W} - q_{ls,o}}{\Delta q_{ls,o}} * 100\% \tag{3}$$

In Equations 2 and 3, the subscript ls denotes the selected lower stratospheric range, m indicates the slope of the linear relationships, q indicates the x-axis tracer mixing ratio at the midpoint of the lower stratospheric range considered (i.e., 418 pptv of CFC-12), and subscripts W and o indicate modeled by WACCM and observed, respectively. The diagnostics in Equations 2 and 3 enable a quantitative evaluation of WACCM's performance at representing the observed tracer relationships, separating the model representation of lower stratospheric dynamics and chemistry from offsets in the absolute mixing ratios found there.

To demonstrate the application of the loss rate and mixing ratio error diagnostics defined here, Figure 9 shows calculated results for the choice of two chemical vertical coordinates and two model domain selections. The selected vertical coordinates are CFC-12 (Figure 8) and N_2O (Figure S4, for which a range of 265-292 ppbv is chosen for the lower stratosphere). The two domain selections are that shown in the gray box in Figure 1 (75-95E, 18-32N; denoted "small"), which is used throughout Sections 3.1 and 3.2, and a larger domain which approximately represents the ASM UTLS anticyclone (30-130E, 18-40N; denoted "large").

The mixing ratio offset diagnostic (Equation 3) shows errors for all species which are less than 20% (Figure 9a), which is conceptually consistent with the stratospheric entry diagnostic presented in Section 3.2 (Figure 6). Indeed, a species with an accurate mixing ratio at the tropopause is predisposed to an accurate mixing ratio in the lower stratosphere. While the loss rate diagnostic (Equation 2; Figure 9b) also shows errors of less than 20% for most relationships, it identifies CFC-114 and CFC-115 as species

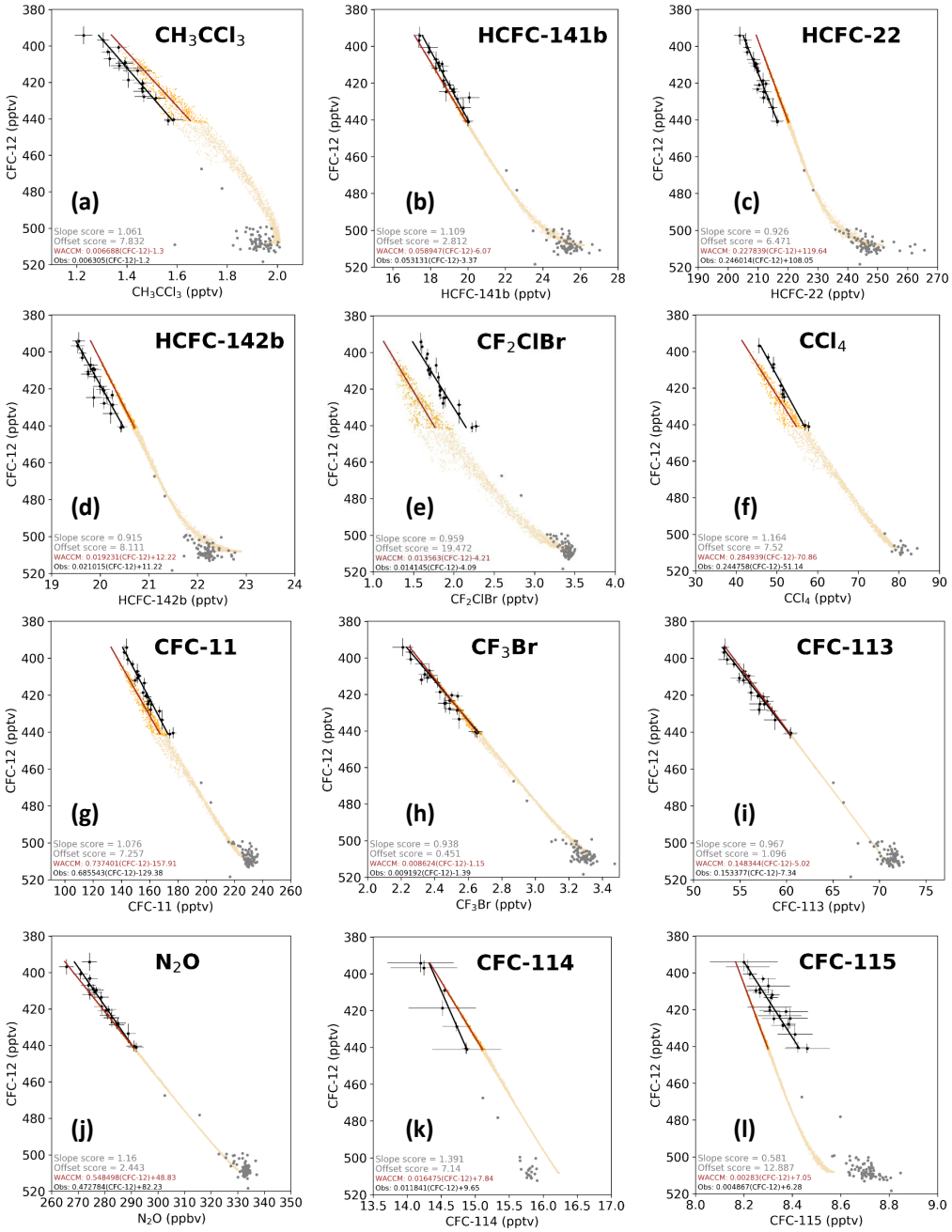

Figure 8. Various halocarbon and N_2O profiles in CFC-12 chemical vertical coordinate space. Black dots show StratoClim observations in the lower stratosphere (394 pptv < CFC-12 < 442 pptv), with thin lines marking observational uncertainty. Thick black lines mark observational best-fits using a weighted linear regression. WACCM is shown in orange, with brown lines marking the linear model best-fit in the lower stratosphere. WACCM is subset between 78-92E, 18-32N (the small gray box in Figure 1), from July 27 - August 10, 2017, to 50-200 hPa to focus on the UTLS, and to every 50th point for visual clarity. Light orange and gray dots show model and observation points (respectively) near and below the tropopause, which are not used for the linear fitting.

with considerable deviations from the observed loss rates in chemical coordinate space. These deviations in loss rate, coupled with their poor stratospheric entry mixing ratio representation (Figure 6), are evidence that WACCM does not properly represent them. For both CFC-114 and CFC-115, loss by O^1D is an important process in comparison to loss by photolysis (from SPARC Report No. 6, 2013), which we highlight using asterisks in the Figure 9 labeling. With this in mind, we find it reasonable to hypothesize that the model ozone high bias noted in Section 3.1 (Figure 3) contributes to the errors in these relationships, as ozone is the main source of O^1D in the lower stratosphere. A subsequent model experiment was performed with a longer spin-up to test for sensitivity in CFC-114 and CFC-115 given their relatively long stratospheric lifetimes, which did not yield improvements to this relationship (not shown).

We clarify again that it is not our objective to make corrections to the chemical mechanisms in the present work, only to show the utility of this diagnostic framework for identifying areas for focused model improvement. Investigating the shortcomings of these relationships are the subject of ongoing work, and may require the use of idealized chemical modeling to understand the complex mechanisms contributing to these relationships.

With the use of the stratospheric mixing ratio offset and chemical loss rate diagnostics in this subsection, we demonstrate that WACCM chemistry overall performs well at representing the chemical relationships observed during StratoClim. As with prior analyses, this diagnostic minimizes the impact of fundamental air mass size disparities between observed and modeled air masses. Both diagnostics show a general consistency between the two choices of chemical vertical coordinate as well as the two choices of domain. The consistency between the two domain choices suggests that the ASM anticyclone has a composition signature in the lower stratosphere that is fairly consistent throughout; despite the StratoClim campaign spanning only a modest portion of the ASM UTLS anticyclone.

4 Conclusions and Outlook

In this study we design a set of process-based diagnostics using airborne in situ chemical tracer measurements to evaluate the representation of UTLS composition under the influence of ASM dynamics and transport. The diagnostics are:

1. The use of tropopause-relative altitude and potential temperature vertical coordinates to evaluate distributions of tropospheric and stratospheric tracers (Section 3.1). These coordinates adjust for dynamical differences between models and the real atmosphere, and allow for the properties of modeled and observed convection to be diagnosed.
2. The use of a tropopause-relative altitude vertical coordinate to evaluate stratospheric entry mixing ratios of chemical species (Section 3.2). For species with tropospheric lifetimes which are long compared to typical tropospheric overturning time scales, this diagnoses the representation of the mixing ratio boundary condition used at the model surface.
3. The use of long-lived tracers as a vertical coordinate to diagnose chemical loss processes in the lower stratosphere (Section 3.3). The application of this to a wide range of species identifies those which may have issues in their chemical treatment by the model.

We demonstrate the application of the above diagnostics in two global climate models run in CTM configuration (WACCM and MUSICA) using airborne in situ observations from the ASM region (StratoClim 2017). The exercise leads to the following conclusions about the representation of ASM composition by WACCM and MUSICA:

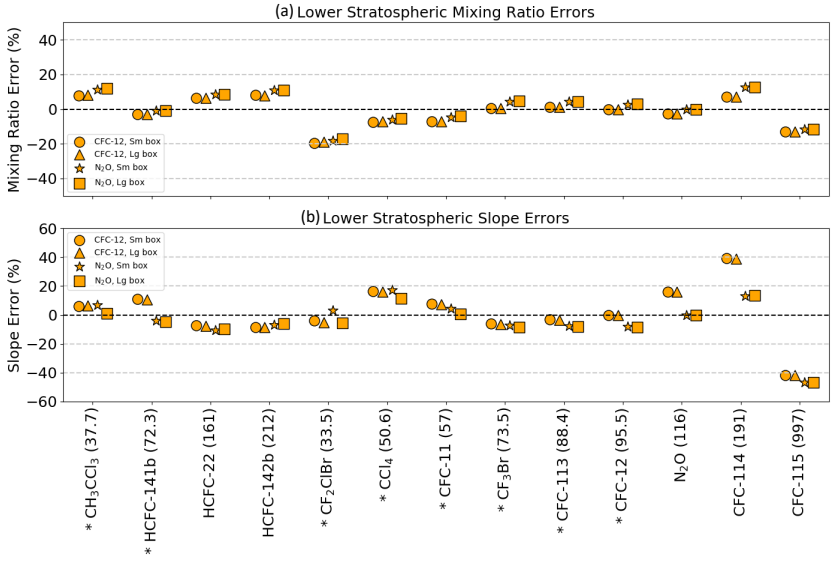

Figure 9. Scatterplots showing (a) mixing ratio errors and (b) loss rate errors between observations and models in the lower stratosphere. Symbols show calculations using CFC-12 and N_2O as the choice of chemical vertical coordinate, as well as two model domain choices (see text for details). Species are organized in the same order as Figure 6, but with their stratospheric lifetimes in years (SPARC Report No. 6) now printed in parentheses instead. Asterisks mark species whose loss is primarily controlled by photolysis.

- The level of ASM deep convective outflow (∼15km; ∼360K) and distribution of CO observed during StratoClim are generally well-represented by WACCM and MUSICA. Both models show similar CO mixing ratios in key altitude ranges, despite differences in their horizontal and vertical grid increments. However, there is a high model bias in ozone throughout the free troposphere.
- Observed tracer mixing ratios at the ASM tropopause are generally consistent with those in WACCM and MUSICA. For species with relatively short tropospheric lifetimes (less than a couple of years), representing mole fraction boundary conditions with a zonal average obscures important regional emissions sources which may lead to large model biases, as shown to be the case for methyl chloride and methyl bromide.
- The use of long-lived chemical vertical coordinates reveals that WACCM represents the compact nature of chemical relationships observed in the lower stratosphere. Species whose stratospheric loss rates are dominated by photolysis have particularly good agreement in their chemical loss rates compared to observations, while the high model ozone bias may negatively impact the representation of loss for other species.

Climate prediction is often conducted on spatial scales of hundreds of kilometers and temporal scales of decades, but accurate prediction at these scales requires accurate representation of embedded smaller-scale processes which are captured by the high spatial and temporal sampling of airborne observations. The diagnostic development and the resulting evaluation of NCAR CESM configurations herein thus highlights the irreplaceable value of airborne observations toward improving Earth system modeling capabilities. Moreover, the diagnostics are designed to minimize the fundamental differ-

ences in air mass sizes represented by models and observations, as compared to a typical method of space-time interpolation.

The establishment of this diagnostic framework may help realize the benefits, and even shortcomings, of ongoing CTM developments. Future work will examine the performance of modeling capabilities at representing a recent set of ASM airborne observations taken during the ACCLIP 2022 campaign (Pan et al., 2022). We note that although these diagnostics are designed specifically with an ASM UTLS focus, we expect them to be appropriate for other regions of the globe to evaluate their respective transport regimes.

5 Open Research

The Community Earth System Model (CESM) is an open-source community model available from http://www.cesm.ucar.edu/. The Whole Atmosphere Community Climate Model (WACCM) is described by https://www2.acom.ucar.edu/gcm/waccm, and the Multi-scale Infrastructure for Chemistry and Aerosols (MUSICA) is described by https://wiki.ucar.edu/display/MUSICA/MUSICA+Home. StratoClim data will be accessible via the HALO database at https://halo-db.pa.op.dlr.de/mission/101. Until this time, it can be provided by request from the respective instrument PIs (see Table 1). SEAC^{4}RS observations are available from https://www-air.larc.nasa.gov/cgi-bin/ArcView/seac4rs. ERA5 reanalysis (doi: 10.5065/P8GT-0R61) is available from the NCAR CISL Research Data Archive.

Acknowledgments

The National Center for Atmospheric Research (NCAR) is supported by the National Science Foundation (NSF). W.P.S. was supported under grant NSF AGS-1853929. K.E.A. was funded by the UK Natural Environment Research Council through the EnvEast Doctoral Training Partnership (grant number NE/L002582/1). We acknowledge high-performance computing support from Cheyenne (https://doi.org/10.5065/D6RX99HX) provided by NCAR's Computational and Information Systems Laboratory (CISL), sponsored by the NSF. Airborne measurements were made possible by European Community's Seventh Framework Programme (FP7/2007–2013), grant agreement 603557—Project STRATOCLIM. We acknowledge support from the Geophysica aircraft team, the StratoClim science team and the NCAR multi-scale modeling community, as well as helpful comments from M. Barth, W. Randel and E. Weatherhead.

References

Adcock, K. E., Fraser, P. J., Hall, B. D., Langenfelds, R. L., Lee, G., Montzka, S. A., ... others (2021). Aircraft-based observations of ozone-depleting substances in the upper troposphere and lower stratosphere in and above the asian summer monsoon. *Journal of Geophysical Research: Atmospheres*, *126*(1), e2020JD033137.

Avallone, L. M., & Prather, M. J. (1997). Tracer-tracer correlations: Three-dimensional model simulations and comparisons to observations. *Journal of Geophysical Research: Atmospheres*, *102*(D15), 19233–19246.

Bednarz, E. M., Hossaini, R., Chipperfield, M. P., Abraham, N. L., & Braesicke, P. (2022). Atmospheric impacts of chlorinated very short-lived substances over the recent past–part 1: Stratospheric chlorine budget and the role of transport. *Atmospheric Chemistry and Physics*, *22*(16), 10657–10676.

Bergman, J. W., Fierli, F., Jensen, E. J., Honomichl, S., & Pan, L. L. (2013). Boundary layer sources for the asian anticyclone: Regional contributions to a vertical conduit. *Journal of Geophysical Research: Atmospheres*, *118*(6),

2560–2575.

Bian, J., Pan, L. L., Paulik, L., Vömel, H., Chen, H., & Lu, D. (2012). In situ water vapor and ozone measurements in lhasa and kunming during the asian summer monsoon. *Geophysical Research Letters*, *39*(19).

Bossolasco, A., Jegou, F., Sellitto, P., Berthet, G., Kloss, C., & Legras, B. (2021). Global modeling studies of composition and decadal trends of the asian tropopause aerosol layer. *Atmospheric Chemistry and Physics*, *21*(4), 2745–2764.

Brunamonti, S., Jorge, T., Oelsner, P., Hanumanthu, S., Singh, B. B., Kumar, K. R., ... others (2018). Balloon-borne measurements of temperature, water vapor, ozone and aerosol backscatter on the southern slopes of the himalayas during stratoclim 2016–2017. *Atmospheric Chemistry and Physics*, *18*(21), 15937–15957.

Bucci, S., Legras, B., Sellitto, P., d'Amato, F., Viciani, S., Montori, A., ... others (2020). Deep-convective influence on the upper troposphere–lower stratosphere composition in the asian monsoon anticyclone region: 2017 stratoclim campaign results. *Atmospheric Chemistry and Physics*, *20*(20), 12193–12210.

Chen, B., Xu, X., Yang, S., & Zhao, T. (2012). Climatological perspectives of air transport from atmospheric boundary layer to tropopause layer over asian monsoon regions during boreal summer inferred from lagrangian approach. *Atmospheric Chemistry and Physics*, *12*(13), 5827–5839.

Clemens, J., Vogel, B., Hoffmann, L., Griessbach, S., Thomas, N., Fadnavis, S., ... Ploeger, F. (2023). Identification of source regions of the asian tropopause aerosol layer on the indian subcontinent in august 2016. *EGUsphere*, *2023*, 1–39.

Danabasoglu, G., Lamarque, J.-F., Bacmeister, J., Bailey, D., DuVivier, A., Edwards, J., ... others (2020). The community earth system model version 2 (cesm2). *Journal of Advances in Modeling Earth Systems*, *12*(2), e2019MS001916.

Dethof, A., O'neill, A., Slingo, J., & Smit, H. (1999). A mechanism for moistening the lower stratosphere involving the asian summer monsoon. *Quarterly Journal of the Royal Meteorological Society*, *125*(556), 1079–1106.

Dubé, K., Randel, W., Bourassa, A., & Degenstein, D. (2022). Tropopause-level nox in the asian summer monsoon. *Geophysical Research Letters*, *49*(18), e2022GL099848.

Dutton, G. S., Hall, B. D., Montzka, S. A., & Nance, J. D. (2023). Combined atmospheric chlorofluorocarbon-12 dry air mole fractions from the noaa gml halocarbons sampling network, 1977-2023. *https://doi.org/10.15138/PJ63-H440*.

Emmons, L., Schwantes, R. H., Orlando, J. J., Tyndall, G., Kinnison, D., & Lamarque, J.-F. e. a. (2020). The chemistry mechanism in the community earth system model version 2 (cesm2). *Journal of Advances in Modeling Earth Systems*.

Fan, Q., Bian, J., & Pan, L. L. (2017). Stratospheric entry point for upper-tropospheric air within the asian summer monsoon anticyclone. *Science China Earth Sciences*, *60*, 1685–1693.

Fernandez, R. P., Barrera, J. A., López-Noreña, A. I., Kinnison, D. E., Nicely, J., Salawitch, R. J., ... others (2021). Intercomparison between surrogate, explicit, and full treatments of vsl bromine chemistry within the cam-chem chemistry-climate model. *Geophysical Research Letters*, *48*(4), e2020GL091125.

Froidevaux, L., Kinnison, D. E., Wang, R., Anderson, J., & Fuller, R. A. (2019). Evaluation of cesm1 (waccm) free-running and specified dynamics atmospheric composition simulations using global multispecies satellite data records. *Atmospheric Chemistry and Physics*, *19*(7), 4783–4821.

Fu, R., Hu, Y., Wright, J. S., Jiang, J. H., Dickinson, R. E., Chen, M., ... Wu, D. L. (2006). Short circuit of water vapor and polluted air to the global stratosphere by convective transport over the tibetan plateau. *Proceedings of the National Academy of Sciences*, *103*(15), 5664–5669.

Fueglistaler, S., Dessler, A., Dunkerton, T., Folkins, I., Fu, Q., & Mote, P. W. (2009). Tropical tropopause layer. *Reviews of Geophysics*, *47*(1).

Gelaro, R., McCarty, W., Suárez, M. J., Todling, R., Molod, A., Takacs, L., ... others (2017). The modern-era retrospective analysis for research and applications, version 2 (merra-2). *Journal of climate*, *30*(14), 5419–5454.

Gettelman, A., Mills, M., Kinnison, D., Garcia, R., Smith, A., Marsh, D., ... others (2019). The whole atmosphere community climate model version 6 (waccm6). *Journal of Geophysical Research: Atmospheres*, *124*(23), 12380–12403.

Granier, C., Darras, S., Denier van Der Gon, H., Doubalova, J., Elguindi, N., Galle, B., ... others (2019). The copernicus atmosphere monitoring service global and regional emissions. *Reading, United Kingdom: Copernicus Atmosphere Monitoring Service. https://doi.org/10.24380/d0bn-kx16*.

Hersbach, H., Bell, B., Berrisford, P., Hirahara, S., Horányi, A., Muñoz-Sabater, J., ... others (2020). The era5 global reanalysis. *Quarterly Journal of the Royal Meteorological Society*, *146*(730), 1999–2049.

Hoffmann, L., & Spang, R. (2022). An assessment of tropopause characteristics of the era5 and era-interim meteorological reanalyses. *Atmospheric Chemistry and Physics*, *22*(6), 4019–4046.

Homan, C., Volk, C., Kuhn, A., Werner, A., Baehr, J., Viciani, S., ... Ravegnani, F. (2010). Tracer measurements in the tropical tropopause layer during the amma/scout-o3 aircraft campaign. *Atmospheric Chemistry and Physics*, *10*(8), 3615–3627.

Honomichl, S. B., & Pan, L. L. (2020). Transport from the asian summer monsoon anticyclone over the western pacific. *Journal of Geophysical Research: Atmospheres*, *125*(13), e2019JD032094.

Kloss, C., Tan, V., Leen, J. B., Madsen, G. L., Gardner, A., Du, X., ... others (2021). Airborne mid-infrared cavity enhanced absorption spectrometer (amica). *Atmospheric Measurement Techniques*, *14*(8), 5271–5297.

Ko, M. K., Newman, P. A., Reimann, S., Strahan, S. E., Atlas, E. L., Burkholder, J. B., ... others (2013). Recommended values for steady-state atmospheric lifetimes and their uncertainties. *SPARC Report on the Lifetimes of Stratospheric Ozone-Depleting Substances, Their Replacements, and Related Species*.

Krishnamurti, T. N., & Bhalme, H. (1976). Oscillations of a monsoon system. part i. observational aspects. *Journal of Atmospheric Sciences*, *33*(10), 1937–1954.

Legras, B., & Bucci, S. (2020). Confinement of air in the asian monsoon anticyclone and pathways of convective air to the stratosphere during the summer season. *Atmospheric Chemistry and Physics*, *20*(18), 11045–11064.

Munchak, L. A., & Pan, L. L. (2014). Separation of the lapse rate and the cold point tropopauses in the tropics and the resulting impact on cloud top-tropopause relationships. *Journal of Geophysical Research: Atmospheres*, *119*(13), 7963–7978.

Pan, L. L., Atlas, E. L., Salawitch, R., Honomichl, S., Bresch, J., Randel, W., ... others (2017). The convective transport of active species in the tropics (contrast) experiment. *Bulletin of the American Meteorological Society*, *98*(1), 106–128.

Pan, L. L., Bowman, K. P., Atlas, E. L., Wofsy, S. C., Zhang, F., Bresch, J. F., ... others (2010). The stratosphere–troposphere analyses of regional transport 2008 experiment. *Bulletin of the American Meteorological Society*, *91*(3), 327–342.

Pan, L. L., Honomichl, S. B., Kinnison, D. E., Abalos, M., Randel, W. J., Bergman, J. W., & Bian, J. (2016). Transport of chemical tracers from the bound-

ary layer to stratosphere associated with the dynamics of the asian summer monsoon. *Journal of Geophysical Research: Atmospheres*, *121*(23), 14–159.

Pan, L. L., Kinnison, D., Liang, Q., Chin, M., Santee, M. L., Flemming, J., ... others (2022). A multimodel investigation of asian summer monsoon utls transport over the western pacific. *Journal of Geophysical Research: Atmospheres*, *127*(24), e2022JD037511.

Park, M., Randel, W. J., Gettelman, A., Massie, S. T., & Jiang, J. H. (2007). Transport above the asian summer monsoon anticyclone inferred from aura microwave limb sounder tracers. *Journal of Geophysical Research: Atmospheres*, *112*(D16).

Park, M., Randel, W. J., Kinnison, D. E., Garcia, R. R., & Choi, W. (2004). Seasonal variation of methane, water vapor, and nitrogen oxides near the tropopause: Satellite observations and model simulations. *Journal of Geophysical Research: Atmospheres*, *109*(D3).

Ploeger, F., Konopka, P., Günther, G., Grooß, J.-U., & Müller, R. (2010). Impact of the vertical velocity scheme on modeling transport in the tropical tropopause layer. *Journal of Geophysical Research: Atmospheres*, *115*(D3).

Ploeger, F., Konopka, P., Walker, K., & Riese, M. (2017). Quantifying pollution transport from the asian monsoon anticyclone into the lower stratosphere. *Atmospheric Chemistry and Physics*, *17*(11), 7055–7066.

Plumb, R. A., & Ko, M. K. (1992). Interrelationships between mixing ratios of long-lived stratospheric constituents. *Journal of Geophysical Research: Atmospheres*, *97*(D9), 10145–10156.

Randel, W. J., Park, M., Emmons, L., Kinnison, D., Bernath, P., Walker, K. A., ... Pumphrey, H. (2010). Asian monsoon transport of pollution to the stratosphere. *Science*, *328*(5978), 611–613.

Schwantes, R. H., Lacey, F. G., Tilmes, S., Emmons, L. K., Lauritzen, P. H., Walters, S., ... others (2022). Evaluating the impact of chemical complexity and horizontal resolution on tropospheric ozone over the conterminous us with a global variable resolution chemistry model. *Journal of Advances in Modeling Earth Systems*, *14*(6), e2021MS002889.

Strahan, S., Duncan, B., & Hoor, P. (2007). Observationally derived transport diagnostics for the lowermost stratosphere and their application to the gmi chemistry and transport model. *Atmospheric Chemistry and Physics*, *7*(9), 2435–2445.

Tang, W., Emmons, L. K., Worden, H. M., Kumar, R., He, C., Gaubert, B., ... others (2023). Application of the multi-scale infrastructure for chemistry and aerosols version 0 (musicav0) for air quality in africa. *Geoscientific Model Development Discussions*, *2023*, 1–34.

Toon, O. B., Maring, H., Dibb, J., Ferrare, R., Jacob, D. J., Jensen, E. J., ... others (2016). Planning, implementation, and scientific goals of the studies of emissions and atmospheric composition, clouds and climate coupling by regional surveys (seac4rs) field mission. *Journal of Geophysical Research: Atmospheres*, *121*(9), 4967–5009.

Ulanovsky, A., Yushkov, V., Sitnikov, N., & Ravengnani, F. (2001). The fozan-ii fast-response chemiluminescent airborne ozone analyzer. *Instruments and Experimental Techniques*, *44*, 249–256.

Viciani, S., Montori, A., Chiarugi, A., & D'Amato, F. (2018). A portable quantum cascade laser spectrometer for atmospheric measurements of carbon monoxide. *Sensors*, *18*(7), 2380.

Villamayor, J., Iglesias-Suarez, F., Cuevas, C. A., Fernandez, R. P., Li, Q., Abalos, M., ... others (2023). Very short-lived halogens amplify ozone depletion trends in the tropical lower stratosphere. *Nature Climate Change*, 1–7.

Vogel, B., Günther, G., Müller, R., Grooß, J.-U., & Riese, M. (2015). Impact of different asian source regions on the composition of the asian monsoon anticy-

clone and of the extratropical lowermost stratosphere. *Atmospheric chemistry and physics*, *15*(23), 13699–13716.

Vogel, B., Müller, R., Günther, G., Spang, R., Hanumanthu, S., Li, D., ... Stiller, G. P. (2019). Lagrangian simulations of the transport of young air masses to the top of the asian monsoon anticyclone and into the tropical pipe. *Atmospheric Chemistry and Physics*, *19*(9), 6007–6034.

von Hobe, M., Ploeger, F., Konopka, P., Kloss, C., Ulanowski, A., Yushkov, V., ... others (2021). Upward transport into and within the asian monsoon anticyclone as inferred from stratoclim trace gas observations. *Atmospheric Chemistry and Physics*, *21*(2), 1267–1285.

Yan, X., Konopka, P., Ploeger, F., Podglajen, A., Wright, J. S., Müller, R., & Riese, M. (2019). The efficiency of transport into the stratosphere via the asian and north american summer monsoon circulations. *Atmospheric Chemistry and Physics*, *19*(24), 15629–15649.

Yin, M. T. (1949). Synoptic-aerologic study of the onset of the summer monsoon over india and burma. *Journal of Atmospheric Sciences*, *6*(6), 393–400.

Yushkov, V., Oulanovsky, A., Lechenuk, N., Roudakov, I., Arshinov, K., Tikhonov, F., ... Georgiadis, T. (1999). A chemiluminescent analyzer for stratospheric measurements of the ozone concentration (fozan). *Journal of Atmospheric and Oceanic Technology*, *16*(10), 1345–1350.

Zhang, G., & McFarlane, N. (1995). Sensitivity of climate simulations to the parameterization of cumulus convection in the canadian climate centre general circulation model. *Atmosphere Ocean*, *33*, 407–446.

Journal of Geophysical Research: Atmospheres

Supporting Information for

Evaluating the Model Representation of Asian Summer Monsoon UTLS Transport and Composition using Airborne In Situ Observations

Warren P. Smith[1], Laura L. Pan[1], Douglas Kinnison[1], Elliot Atlas[2], Shawn Honomichl[1], Jun Zhang[1], Simone Tilmes[1], Rafael P. Fernandez[3], Alfonso Saiz-Lopez[4], Victoria Treadaway[5,6], Karina E. Adcock[7], Johannes C. Laube[8], Marc von Hobe[8], Corinna Kloss[8], Silvia Viciani[9], Francesco D'Amato[9], C. Michael Volk[10], Fabrizio Ravegnani[11]

1 Atmospheric Chemistry Observations & Modeling Laboratory, National Center for Atmospheric Research, Boulder, Colorado, USA
2 Department of Atmospheric Sciences, Rosenstiel School of Marine, Atmospheric, and Earth Science, University of Miami, Miami, Florida, USA
3 Institute for Interdisciplinary Science (ICB), National Research Council (CONICET), FCEN-UNCuyo, Mendoza, Argentina
4 Department of Atmospheric Chemistry and Climate, Institute of Physical Chemistry Blas Cabrera, CSIC, Madrid, Spain
5 Cooperative Institute for Research in Environmental Sciences, University of Colorado Boulder, Boulder, Colorado, USA
6 NOAA Chemical Sciences Laboratory, Boulder, Colorado USA
7 Centre for Ocean and Atmospheric Sciences, School of Environmental Sciences, University of East Anglia, Norwich, United Kingdom
8 Institute for Energy and Climate Research (IEK-7), Forschungszentrum Jülich GmbH, 52425 Jülich, Germany
9 National Research Council - National Institute of Optics (CNR-INO), Sesto Fiorentino, Italy
10 University of Wuppertal, Wuppertal, Germany
11 Institute of Atmospheric Sciences and Climate, Bologna, Italy

Contents of this file

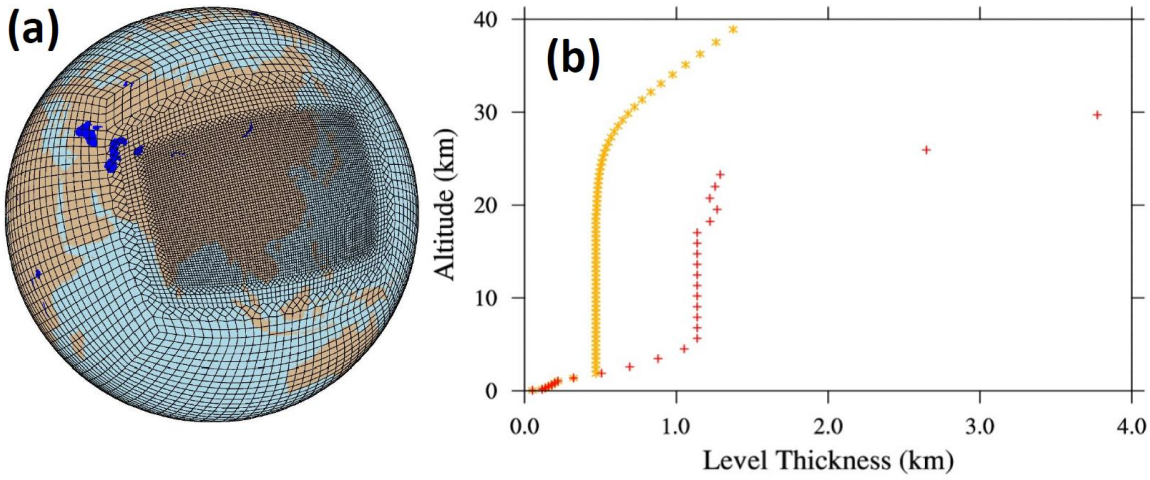

Figure S1: (Left) An image depicting the horizontal grid structure for the MUSICA simulation analyzed herein. This grid mesh was originally developed for forecasting application during an airborne field campaign, the Asian summer monsoon Chemical and Climate Impact Project (ACCLIP), which took place in summer 2022. (Right) The thickness of each model layer in the analyzed (orange, 110 total levels) WACCM and (red, 32 total levels) MUSICA simulations.

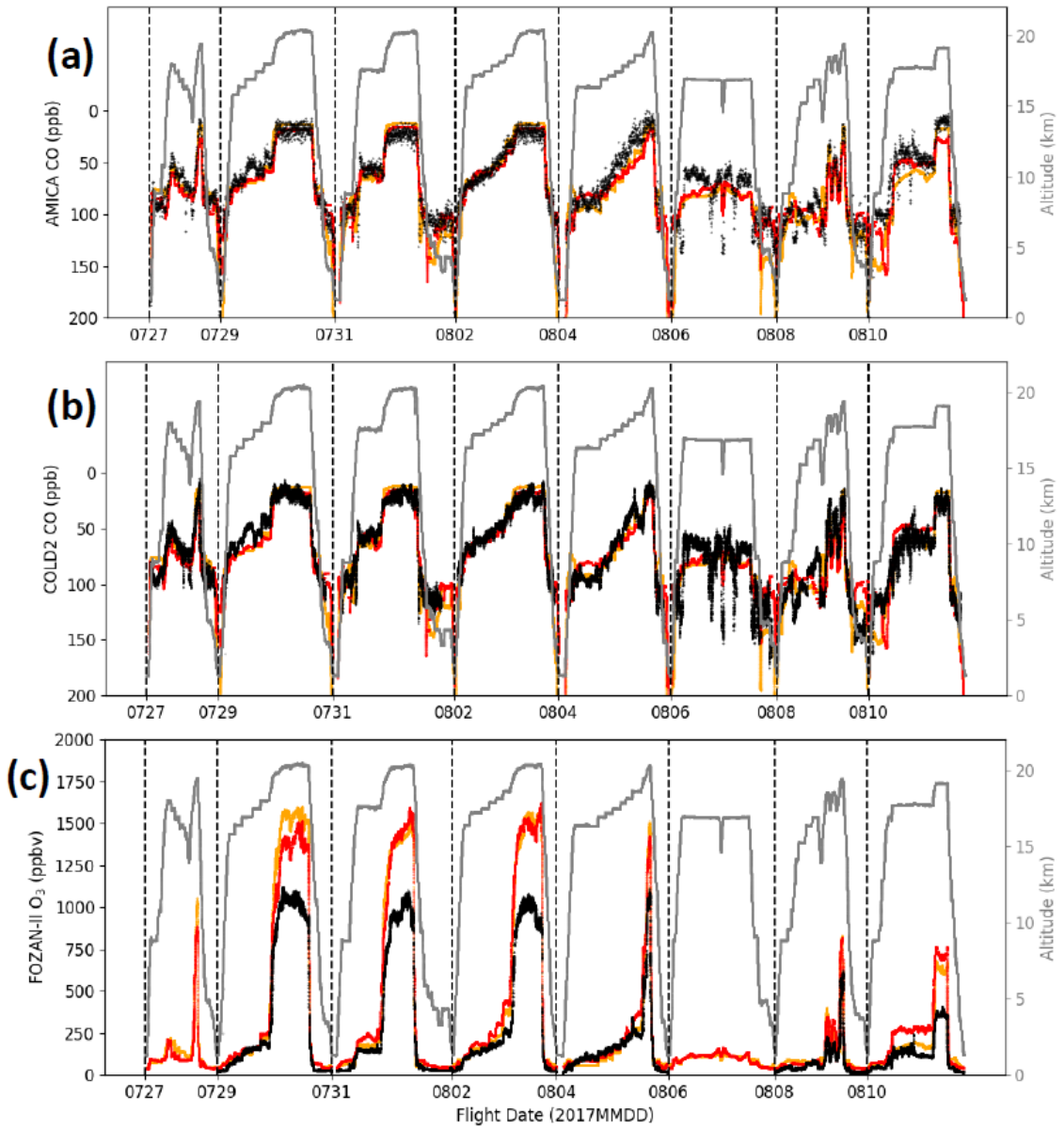

Figure S2: Time series of observed and model CO and ozone mixing ratios interpolated in space and time to StratoClim flight tracks from the (red) MUSICA and (orange) WACCM simulations. Black dots show (a) AMICA CO, (b) COLD2 CO and (c) FOZAN-II ozone. Gray lines show the aircraft altitude. Note y-axes for CO are flipped.

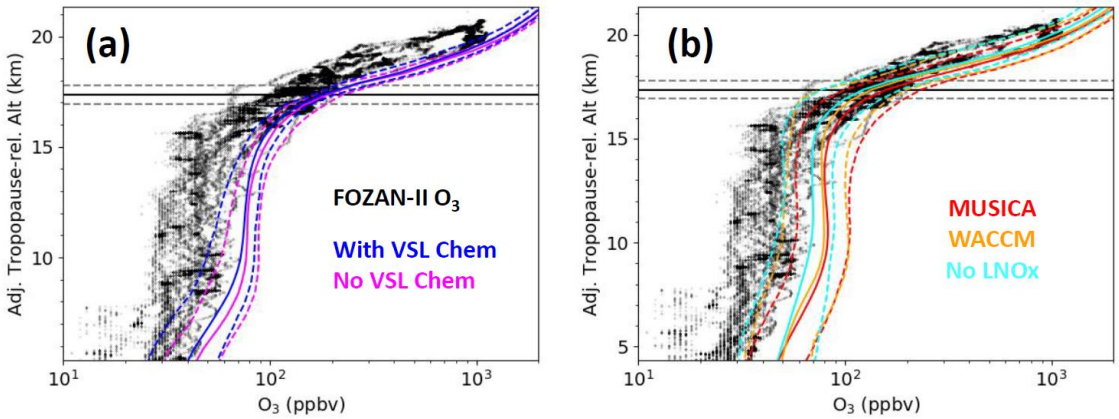

Figure S3: As in Figure 3, but for sensitivity runs which explore the model ozone high bias, and with dashed lines to indicate the 5th and 95th percentiles for the models. The left panel shows sensitivity runs for the inclusion of very short-lived (VSL) chemistry. We note that these are free-running simulations with prescribed SSTs which are not nudged to analysis like the WACCM and MUSICA runs in this study, they are only used to assess the relative impact of VSL chemistry. The right panel shows sensitivity to a CAM-Chem simulation (in cyan) where lightning NOx production is disabled.

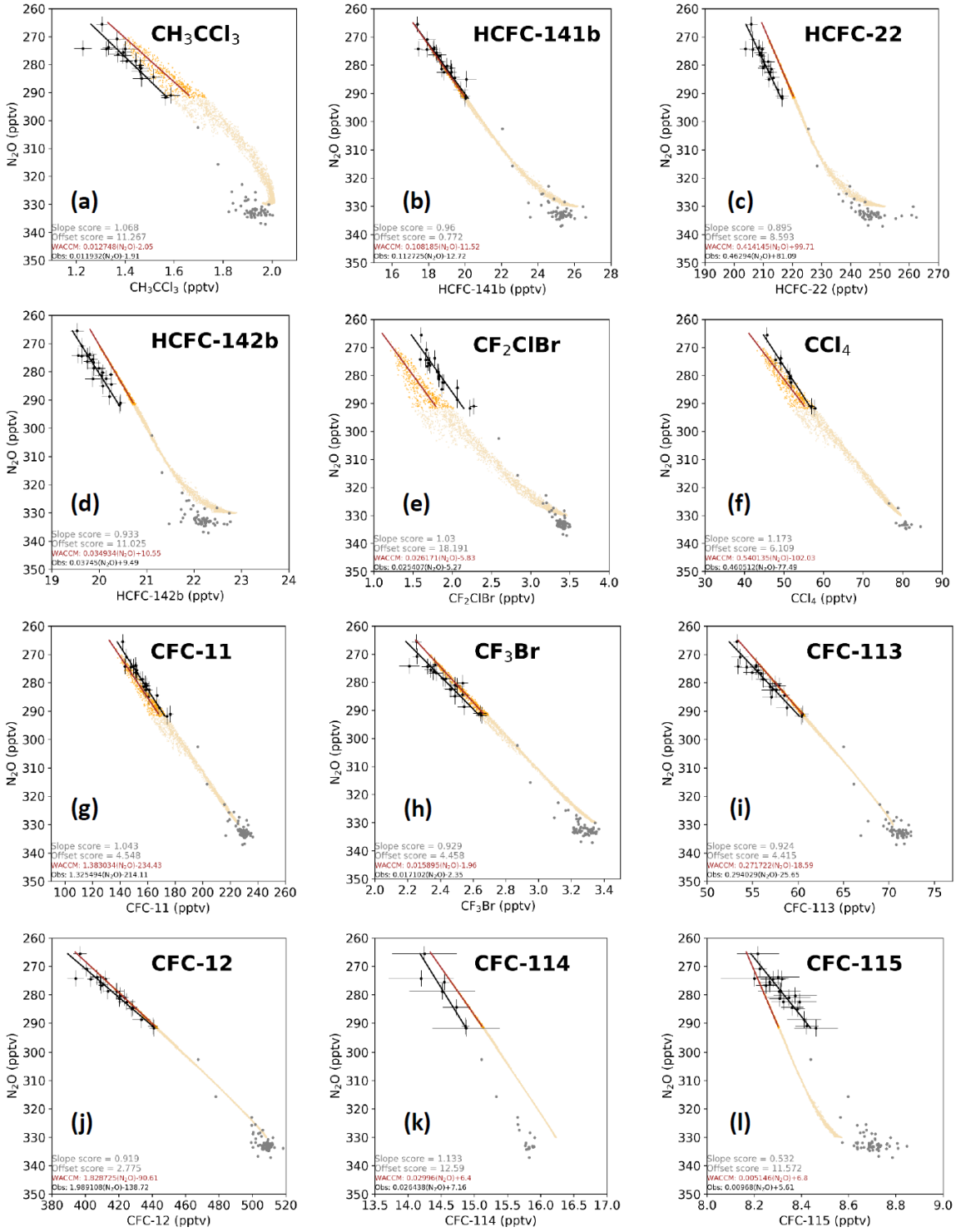

Figure S4: As in Figure 8, but using N_2O as the chemical vertical coordinate.